International Journal of Earth Sciences (2022) 111:2317–2335
https://doi.org/10.1007/s00531-022-02223-z

ORIGINAL PAPER

Petrogenesis and tectonic setting of Early Silurian island-arc-type quartz diorite at the southern margin of the East Kunlun orogenic belt: analysis of the evolution of the Proto-Tethyan Ocean

Zuochen Li[1,2] · Xianzhi Pei[1] · Ruibao Li[1] · Paul D. Bons[3,2] · Lei Pei[1] · Youxin Chen[1] · Chengjun Liu[1] · Meng Wang[1] · Shaowei Zhao[1] · Guochao Chen[4] · Hai Zhou[1] · Jie Zhao[1] · Lili Xu[1] · Hao Lin[1] · Irshad Hussain[1]

Received: 18 December 2021 / Accepted: 29 June 2022 / Published online: 30 July 2022

Abstract

The subduction of the Proto-Tethyan Ocean is still a controversial subject. Here we report zircon U-Pb ages, geochemistry, and Hf isotopic compositions of the zircon in the Mengkete quartz diorite in the Buqingshan–A'nyemaqen Tectonic Mélange Belt, which lies at the southern margin of the East Kunlun orogenic belt on the northern Tibetan Plateau, to constrain the petrogenesis of subduction-related granitoids and to reconstruct the evolution of the Buqingshan–A'nyemaqen Ocean. Zircons U-Pb dating yields coeval ages of 441–436 Ma for Mengkete quartz diorite. Mengkete plutons have variable SiO_2 (56.63–65.22%) and high Al_2O_3 (16.09–17.79%) contents and aluminous saturation indexes (A/CNK ratios) ranging from 0.77 to 0.96, which define their metaluminous and medium-K_2O calc-alkaline signatures. The plutons have a low total rare-earth element (REE) content (45.49–168.31 ppm) and slightly positive Eu anomalies (Eu/Eu* in the range of 0.96 to 1.32). They are also enriched in large-ion lithophile elements (LILEs), such as Rb, Th, and Ba, but are depleted in high-field-strength elements (HFSEs), such as Nb, Ta, Zr, Hf, and Ti. Their zircon $\varepsilon_{Hf}(t)$ values ranging from 7.79 to 13.02, and the two-stage Hf (T_{DM2}) model ages are in the range of 1130–657 Ma. These geochemical signatures indicate that the Mengkete quartz diorite was derived from partial melting of the mafic Meso-Neoproterozoic lower crust during the northward subduction of the Proto-Tethyan Ocean. The evolution of the East Kunlun Belt can be divided into five stages from the Neoproterozoic to late Middle Triassic: (1) an opend Buqingshan−A'nyemaqen ocean during the Neoproterozoic up to 516Ma; (2) the continuous expansion of the Buqingshan−A'nyemaqen ocean during the period 516 to 441Ma, along with the beginning of northward subduction in the Late Cambrian; (3) further subduction from 441 to 400Ma, accompanied by the production of large volumes of arc magmatic rocks; (4) the long period during which the Buqinshan–A'nyemaqen Ocean existed (400–240 Ma); and (5) the final closure of the Buqinshan–A'nyemaqen Ocean in the late Middle Triassic.

Keywords Zircon U-Pb dating · Early Silurian · Buqingshan–A'nyemaqen tectonic mélange belt · Proto-Tethyan Ocean

✉ Xianzhi Pei
peixzh@163.com

Zuochen Li
lizuochen2003@163.com

[1] Key Laboratory of Western China's Mineral Resources and Geological Engineering, Ministry of Education, Key Laboratory for the Study of Focused Magmatism and Giant Ore Deposits, Ministry of Natural Resources, School of Earth Science and Resources, Chang'an University, No.126 South of Yanta Road, Yanta District, Xi'an 710054, China

[2] Department of Geosciences, Eberhard Karls University Tübingen, 72074 Tübingen, Germany

[3] School of Earth Sciences and Resources, China University of Geosciences, Beijing 100083, China

[4] School of Civil Engineering, Nanyang Institute of Technology, Nanyang 473000, China

Introduction

The Buqingshan–A'nyemaqen tectonic mélange belt (BTMB) is located at the junction of the East Kunlun, West Qinling and Bayan Har orogenic belt (Fig. 1a, b). The BTMB intersects with the northeastern margin of the Qinghai–Tibet Plateau and the central orogenic system of China and constitutes a significant structural element in which the Proto-Tethyan and Paleo-Tethyan domain are interwoven (Jiang et al. 1992; Bian et al. 1997, 2001; Xu et al. 1996, 2007, 2013; Pei 2001; Wang and Yang 2004; Zhang et al. 2004; Mu et al. 2018; Chen et al. 2020; Li et al. 2020, 2021). Therefore, this region is of great significance to geodynamic research and is well known to be of multistage evolution. It thus provides a natural laboratory for understanding the evolution of the North China Block and the Yangtze Block (Jiang et al. 1992; Xu et al. 1996, 2001; Yin and Zhang 1997; Pan et al. 2012).

Most researchers consider the BTMB to consist of the residual oceanic crust from the closure of the northernmost branch of Late Paleozoic Paleo-Tethyan Ocean at the southern margin of the East Kunlun orogenic belt (EKOB) (Jiang et al. 1992; Xu et al. 2001; Bian et al. 2001; Zhu et al. 2002; Chen et al. 2001; Zhang et al. 2004; Wang and Yang 2004; Wang et al. 2004; Mo et al. 2007; Yang et al. 2009). However, recent studies have suggested that the BTMB also includes an Early Paleozoic island-arc-type magmatic rocks

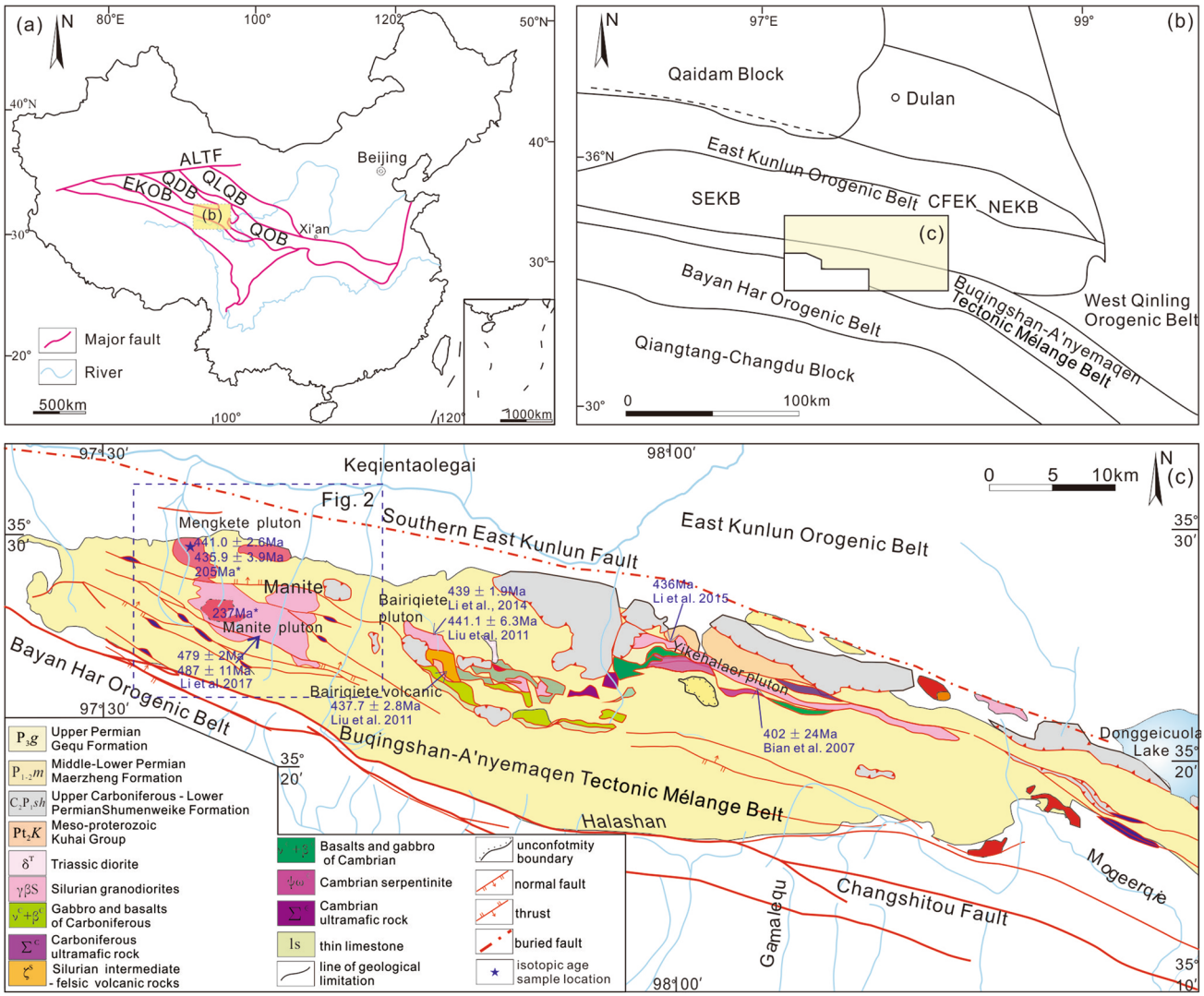

Fig. 1 **a** Map showing the macroscopic tectonic framework of Central Orogenic Belt, China; **b** Simplified tectonic map of western China, showing major tectonic units; Distribution of the Buqingshan Tectonic mélange belt (BTMB); **c** Distribution of Mengkete quartz diorite (rock mass) in the BTMB, southern margin of the EKOB (geological map modified from Yin and Zhang 2003). *NEKB*, Northern East Kunlun Block; *SEKB*, Southern East Kunlun Block; *CFEK*, Central fault of East Kunlun; the age with "*" is from Yin and Zhang (2003)

(Bian et al. 1999a, b, 2007; Li et al. 2017) and ophiolites (Bian et al. 2001, 2004; Liu 2011), indicating that the BTMB underwent subduction and collision during the Early and Late Paleozoic (Zhang et al. 1999, 2000; Liu et al. 2011a, b).

The timing of the closure of the Proto-Tethyan Ocean and the evolution of the EKOB are currently explained by two different models. One model advocates that the closure of the Proto-Tethyan Ocean suggests a northward subduction during the Late Silurian and Devonian (Bian et al. 2004; Liu et al. 2012; Xiong et al. 2015). The alternative model suggests that the Proto-Tethys Ocean did not close in the Early Paleozoic but that the Buqingshan–A'nyemaqen Ocean Basin was closed by the Middle Triassic (Pan et al. 2012; Dong et al. 2018; Pei et al. 2018).

Previous research on the Early Paleozoic magmatic rocks in the region showed that magmatism occurred in two phases. The early phase (Cambrian to Early Ordovician) produced the De Dur'ngoi diorite (Li et al. 2007) and the Manite granodiorite (Li et al. 2017), among other plutonic rocks. The products of the later phase (Early Silurian) include the Yikehalaer, Bairiqiete, and Manite granodiorite, as well as felsic volcanic rocks (e.g., Bian et al. 1999a, b, 2007; Liu 2011; Liu et al. 2011a, b; Li et al. 2014a, b, 2015, 2017). These Early Paleozoic magmatic rocks provided a means of studying the evolution of the Proto-Tethyan Ocean while also presenting the scientific challenge of elucidating which dynamic background might be represented by the two periods of magmatism.

Previous researchers have disputed the age of the plutons found in the Manite area (Qinghai Geological Bureau 1972; Yin and Zhang 2003; Li et al. 2017). It was earlier considered that all of the plutons in the Manite area were formed in the Late Paleozoic (Qinghai Geological Bureau, 1972). Later, Yin and Zhang (2003) divided the Manite plutons into a southern granodiorite pluton and northern quartz diorite pluton, with the southern pluton being formed in the Early Triassic (zircon U-Pb date, 237 Ma) and the northern pluton being formed in the Late Triassic (zircon U-Pb date, 205 Ma). However, Li et al. (2017) dated the southern Manite granodiorite at 487 ± 11 Ma and 479 ± 2 Ma (by zircon U-Pb dating) and proposed that the ongoing subduction of the Proto-Tethyan Ocean in the Buqingshan area during 487–479 Ma formed these Late Cambrian to Early Ordovician island-arc-type granitoids. Field Geological mapping indicates that the northern quartz diorite pluton (the Mengkete) has a fault contact with the surrounding geological units (Fig. 2). Therefore, determination of the formation and the petrogenesis of the Mengkete quartz diorite are of important to understand the evolution of the Proto-Tethyan Ocean and the Paleo-Tethyan Ocean.

In this paper, we focus on Mengkete quartz diorites in the BTMB and present their petrology together with zircon U-Pb-Hf geochronological and geochemical data. Petrogenesis, magma sources, including magma mixing are also discussed with the aim of providing better constraints on the subduction of the Proto-Tethyan Ocean at the southern margin of the EKOB.

Geological setting

The BTMB consists of a discontinuous E–W trending belt that is more than 700 km long and approximately 10–20 km wide (Fig. 1a, b). It stretches from Maqin in the east across Majixueshan and Tuosuohu to Buqingshan and southeast Heicigou (Fig. 1a) to connect with the mafic–ultramafic rocks of Muzitage (Molnar et al. 1987; Burchfiel et al. 1989; Bian et al. 2004, Fig. 1c). To the north, the BTMB is separated from the EKOB and West Qinling orogenic belt by the southern East Kunlun Fault. To the south, it is separated from the Bayan Har orogenic belt by the Changshitou Fault. Forming a suture zone between the Bayan Har and East Kunlun Blocks, the BTMB is a product of the ocean–continent subduction–collision two-phase tectonic evolution during the Early Paleozoic to the Late Paleozoic (Zhang et al. 1999) and belongs to the East Tethyan Ocean tectonic domain (Jiang et al. 1992; Bian et al. 1999a, b, 2001; Chen and Sun 1999; Chen et al. 2001, 2004; Zhu et al. 1999; Yang et al. 2004; Guo et al. 2007; Liu et al. 2011a, b, c; Pei et al. 2018).

The BTMB is composed of the Lower–Middle Permian Maerzheng Formation ($P_{1\text{-}2}m$), which consists of Early Palaeozoic and Late Palaeozoic ophiolites, Palaeozoic rocks, seamount basalts, and limestone (Liu et al. 2011b; Li et al. 2013c, 2014b, 2017; Li et al. 2014a, 2015; Yang et al. 2014; Pei et al. 2015, 2018; Yang et al. 2016; Pei et al. 2017). The Middle Proterozoic Kuhai Group (Pt_2K) found in the northern part of the ophiolite belt includes marble, biotite–quartz schist, gneiss, and amphibolite and constitutes the metamorphic basement. A nappe composed of the Upper Carboniferous to Lower Permian Shumenweike Formation ($C_2P_{1\text{-}2}sh$), which primarily consists of carbonates with apparent reef affinities (Fig. 2), covers the entire area.

The Mengkete quartz diorite is a composite pluton that outcrops in the Manite area and Mengkete Valley in the Buqingshan area (Fig. 2). It is exposed at the surface as two main blocks oriented in an NNW–SEE direction (Fig. 2), occupying an area of ~ 16 km^2. The pluton is in fault contact with the middle to Lower Permian Maerzheng Formation ($P_{1\text{-}2}m$) and the Late Cambrian to Early Ordovician Manite granodiorite (Fig. 2). On the basis of the field geological mapping, we consider that the plutons are allochtonous that form a mélange block within the Maerzheng Formation (Fig. 2). The edge of the intrusive body is strongly gneissic, but both the margin and interior of the block of plutons exhibit a weak deformation (Fig. 3a, b).

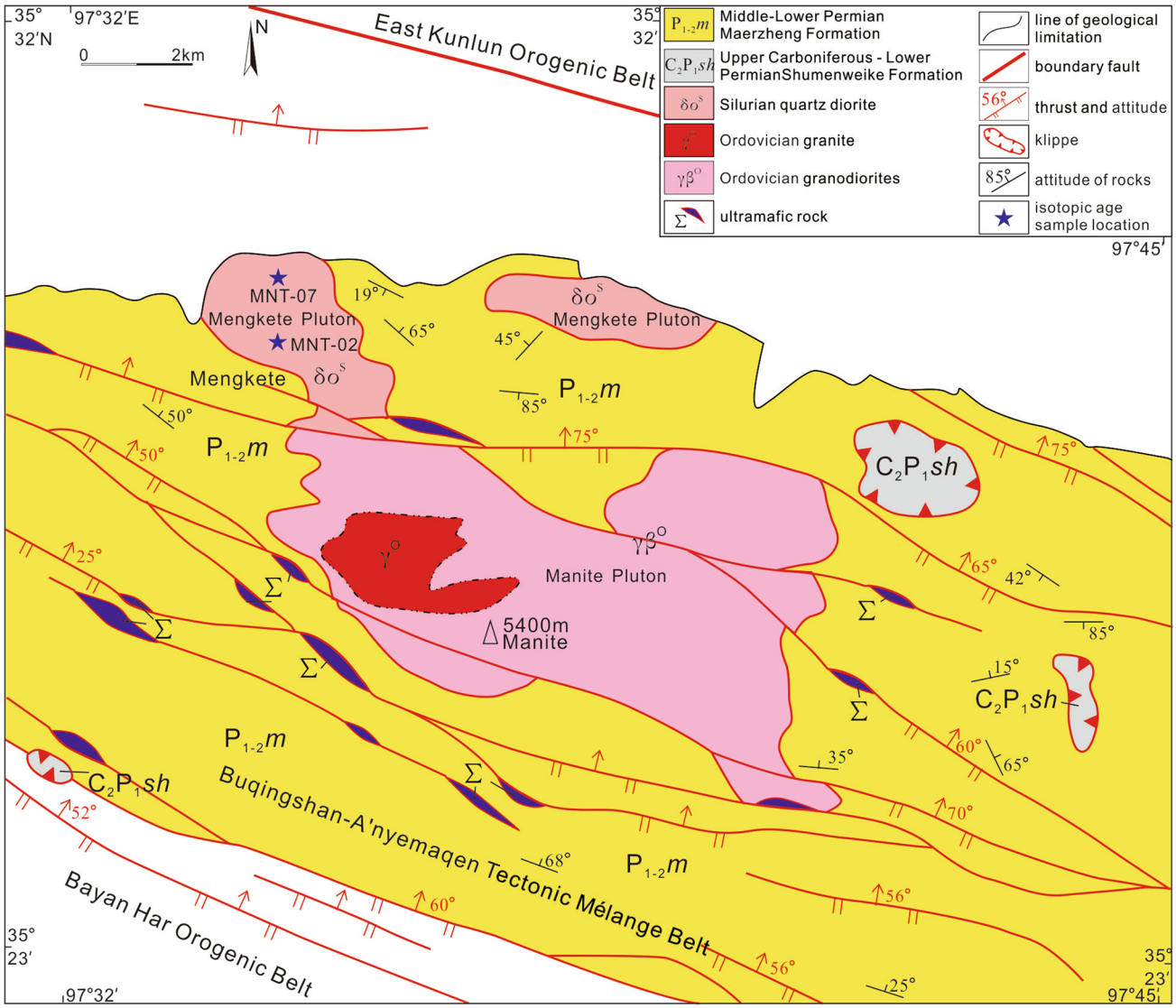

Fig. 2 Simplified geological map of the Mengkete region in BTMB, southern margin of the EKOB (geological map modified from Yin and Zhang 2003)

Petrography

The massive to slightly gneissic diorite is gray to dark gray, with medium-to-fine subhedral grains. The constituent phases are plagioclase (60–65%), quartz (10–18%), amphibole (13–20%), K-feldspar (2–5%), and biotite (1–3%). The accessory minerals are mainly magnetite, titanite, apatite and zircon. The feldspar grains are 0.25–5 mm in size, are subhedral, and show obvious polysynthetic twinning (Fig. 3c, d), and they also exhibit brittle deformation. The quartz grains are 0.1–0.3 mm in size and exhibit undulose extinction (Fig. 3d). The amphibole grains are aligned, and there are some quartz crystals enclosed within the amphibole crystals. The alteration of the diorite occurred mainly by the sericitization and kaolinization of the plagioclase and chloritization of the amphibole and biotite.

Analytical methods

LA-ICP-MS testing

Two quartz diorite samples (MNT-02, MNT-07) from the Mengkete pluton were used for isotopic dating. The geographic coordinates of the samples determined by GPS were 35°28′52.86″N, 97°34′31.32″E, 4408 meters in height, 35°29′35.40″N, 97°34′31.02″E, 4338 meters in height, respectively. Rock specimens were crushed (80–100 mesh) using conventional methods and minerals were

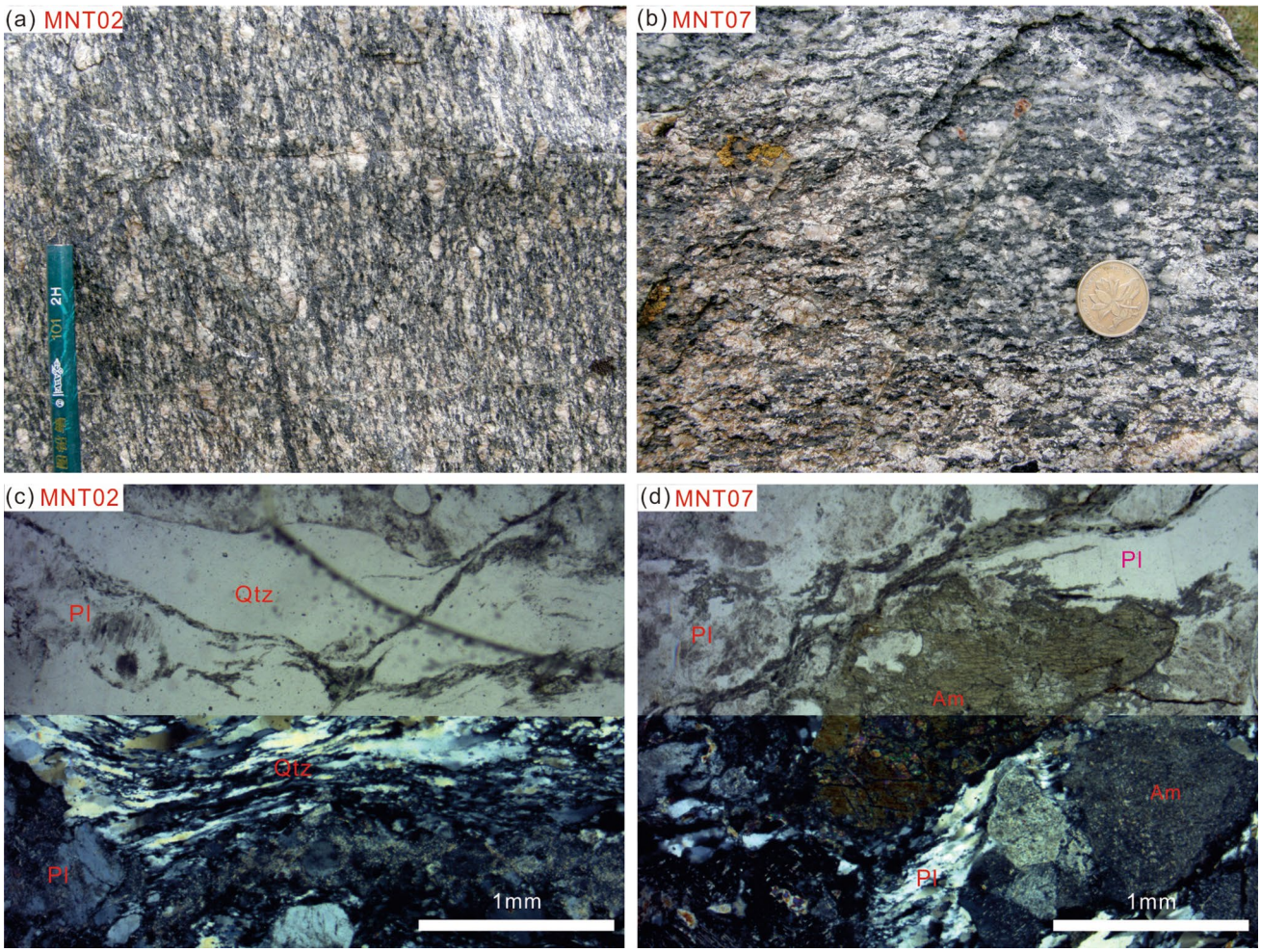

Fig. 3 **a**, **b** Field photographs (viewing toward SE); **c**, **d** microscope micrographs (crossed polarizers, 5 times) of the Mengkete quartz diorite in the BTMB, southern margin of the EKOB. *Am* Amphibole, *Pl* Plagioclase, *Qtz* Quartz

separated by flotation and electromagnetism techniques. Well-formed, crystal-shaped, and transparent zircons were handpicked using a binocular microscope. The zircon grains were mounted on two-sided adhesive tape and fixed with colorless transparent epoxy resin until fully solidified. The surface was polished to expose the interior of the zircons. Cathodoluminescence (CL) microphotographic images were taken with a Cameca electron probe X-ray microanalyser at the Institute of Geology and Geophysics, Chinese Academy of Sciences, Beijing. The analysis voltage was 15 kV, and the current was 19 nA. The *in situ* U-Pb isotopic age analyses of zircons were performed using LA-ICP-MS at the State Key Laboratory of Continental Dynamics, Northwest University, Xi'an. The analysis instruments were an Elan 6100DRC Type Quadrupole Perch Mass Spectrograph and a Geolas 200M excimer laser ablation system (193 nm, Geolas 200M, Lambda Physic). The facula beam diameter of laser ablation was 30 μm, and the depth of laser ablation samples was 20–40 μm. The detailed experimental principles, technological process, and instrumentation parameters used were the same as those reported by Yuan et al. (2003, 2004).

The international standard zircon 91500 was used as an external standard for the calculation of zircon ages. The artificial synthetic silicate glass NIST SRM610, American National Standard Substance Bureau, was adopted as an external standard for element content analysis. ^{29}Si was used as the internal standard element. The isotopic ratio and element content data were analyzed using the GLITTER software (ver. 4.0, Macquarie University). The general lead adjustment was conducted using the Andersen software (Andersen 2002), and ISOPLOT software (3.0 edition, Ludwig 2003) was used for the age calculation and concordia diagrams.

Geochemical analyses

Seven samples were selected for the analyses of major and trace elements. The samples were ground to 200 mesh, and

the major and trace elements were measured in the State Key Laboratory of Lithosphere Evolution, Institute of Geology and Geophysics, Chinese Academy of Sciences. The major elements were tested using X-ray fluorescence spectrometry (XRF-1500). To determine the oxide content, a sheet glass made of 0.5 g sample and 5 g lithium tetraborate was tested using the Shimadzu XRF-1500 with a precision of >2–3%. Trace and rare-earth elements (REE) were analysed by ICP-MS (Element II). The samples were prepared using the acid-solubility method, which has an analytic precision of > 10% (according to the national standards GSR-1 and GSR-2); however, the precision is > 5% when the element content is > 10 ppm. The detailed analysis methods were described by Chen et al. (2000, 2002a).

Zircon Lu-Hf isotope analyses

In situ zircon Hf isotopic analyses were conducted using a Neptune MC-ICPMS, equipped with a 193 nm laser, at the State Key Laboratory of Continental Dynamics, Northwest University, China. During the analyses, a laser repetition rage of 10 Hz at 100 mJ was used and spot diameter was 30 lm. Raw counts for ^{172}Yb, ^{173}Yb, ^{175}Lu, ^{176}(Lu + Yb + Hf), ^{177}Hf, ^{178}Hf, ^{179}Hf, ^{180}Hf and ^{182}W were collected and isobaric interference corrections for ^{176}Lu and ^{176}Yb on ^{176}Hf need to be precisely determined. ^{176}Lu was calibrated using the ^{175}Lu value and correction of ^{176}Yb on ^{176}Hf (Iizuka and Hirata 2005; Iizuka et al. 2017). The detailed analytical technique was described by Yuan et al. (2008). The notations of $\varepsilon_{Hf}(t)$, $f_{Lu/Hf}$, T_{DM1} and T_{DM2} are defined as the same as those in Wu et al. (2007).

Analytical results

Zirocn U-Pb ages

The zircons in the sample MNT-02 of the Mengkete quartz diorite are euhedral and pale yellow to colorless. In cathodoluminescence images (Fig. 4a), these zircons show oscillatory zoning, which is indicative of a magmatic origin (Belousova et al. 2002; Wu and Zheng 2004; Siebel et al. 2005). The zircon is prismatic in form with lengths ranging from 110 to 220 μm and aspect ratios of 1:1–3:1. The thorium and uranium concentrations obtained from the analyses of 24 zircon samples were within the ranges 60.50–455.89 and 160.25–469.25 ppm, respectively (Table S1, in the Supplemental material), and all of the zircons were found to have high Th/U ratios (0.28–1.00) (Table S1, Fig. 5a). All the Th/U ratios were greater than 0.1, and Th and U were positively correlated. The zircons display left-inclined curves in chondrite-normalized REE patterns (Fig. 5b), indicate fractionation between light and heavy rare-earth elements (LREEs and HREEs) evident from positive Ce anomalies (Ce/Ce* = 1.17–148.77) and negative Eu anomalies (Eu/Eu* = 0.41–0.63) (Table S2). All of the zircon Th/U ratios, crystal shapes, and REE patterns indicate that the zircons are of magmatic origin. Samples from 23 of the sample locations—the exception being MNT-0q62-11—indicated concordant ages. The ^{206}Pb/^{238}U ages range from 450 to 426 Ma (Table S1, Fig. 4a), with an average age of 441.0 ± 2.6 Ma (MSWD = 1.7) (Fig. 6a, b), which implies crystallization Early Silurian for the Mengkete quartz diorite.

The zircons in the sample MNT-07 of the Mengkete quartz diorite are euhedral and pale yellow to colorless. In cathodoluminescense images (Fig. 4b), these zircons show oscillatory zoning, which is again indicative of a magmatic origin (Belousova et al. 2002; Wu and Zheng 2004; Siebel et al. 2005). The thorium and uranium concentrations for the 30 zircon samples were within the ranges 69.96–463.19 and 152.46–677.44 ppm, respectively, and all of the zircons were found to have high Th/U ratios (0.44–1.00). All of the Th/U ratios were greater than 0.1, and Th and U were positively correlated (Table S1, Fig. 5c). The zircons display left-inclined curves in chondrite-normalized REE patterns (Fig. 5d) and indicate fractionation between LREEs and HREEs evident from positive Ce anomaly (Ce/Ce* = 1.29–68.38) and negative Eu anomaly (Eu/Eu* = 0.23–0.75) (Table S2). All of the zircon Th/U ratios, crystal shapes, and REE patterns indicate that the zircons are of magmatic origin. Samples from 29 of the sample locations—the exception being MNT-07-007—indicated concordant ages. These ages can be subdivided into two groups: one group (corresponding to 5 of the zircon cores) yielded ^{206}Pb/^{238}U ages ranging from 495 to 465 Ma (Fig. 4b) with a weighted mean age of 474 ± 15 Ma (MSWD = 2.5) (Fig. 6c, d), representing zircons captured from the wall rock. The other group (corresponding to 24 of the samples in zircon rims) yielded ^{206}Pb/^{238}U ages ranging from 450 to 417 Ma (Table S1, Fig. 6c) with a weighted mean age of 435.9 ± 3.9 Ma (MSWD = 0.52) (Fig. 6e); this age corresponds to the crystallization age of the Mengkete quartz diorite. Therefore, we suggest that the Munkte quartz diorite was formed between 441.0 and 435.9 Ma, during the Early Silurian.

Geochemcial characteristics

The SiO_2 content of the Mengkete quartz diorite samples is variable (56.63–65.22%) (Table S3). In a total alkali–silica diagram (Fig. 7a), most of the samples fall into the diorite field and have a low alkali contents (4.91–5.59%) and K_2O/Na_2O ratios of 0.17–0.31. All of the samples can be classified as medium-K calc-alkaline and are characterized by a medium K_2O content and high Al_2O_3 (and low FeO/(FeO + MgO) ratios (16.09–17.79% and 0.49–0.53, respectively) (Fig. 7b).

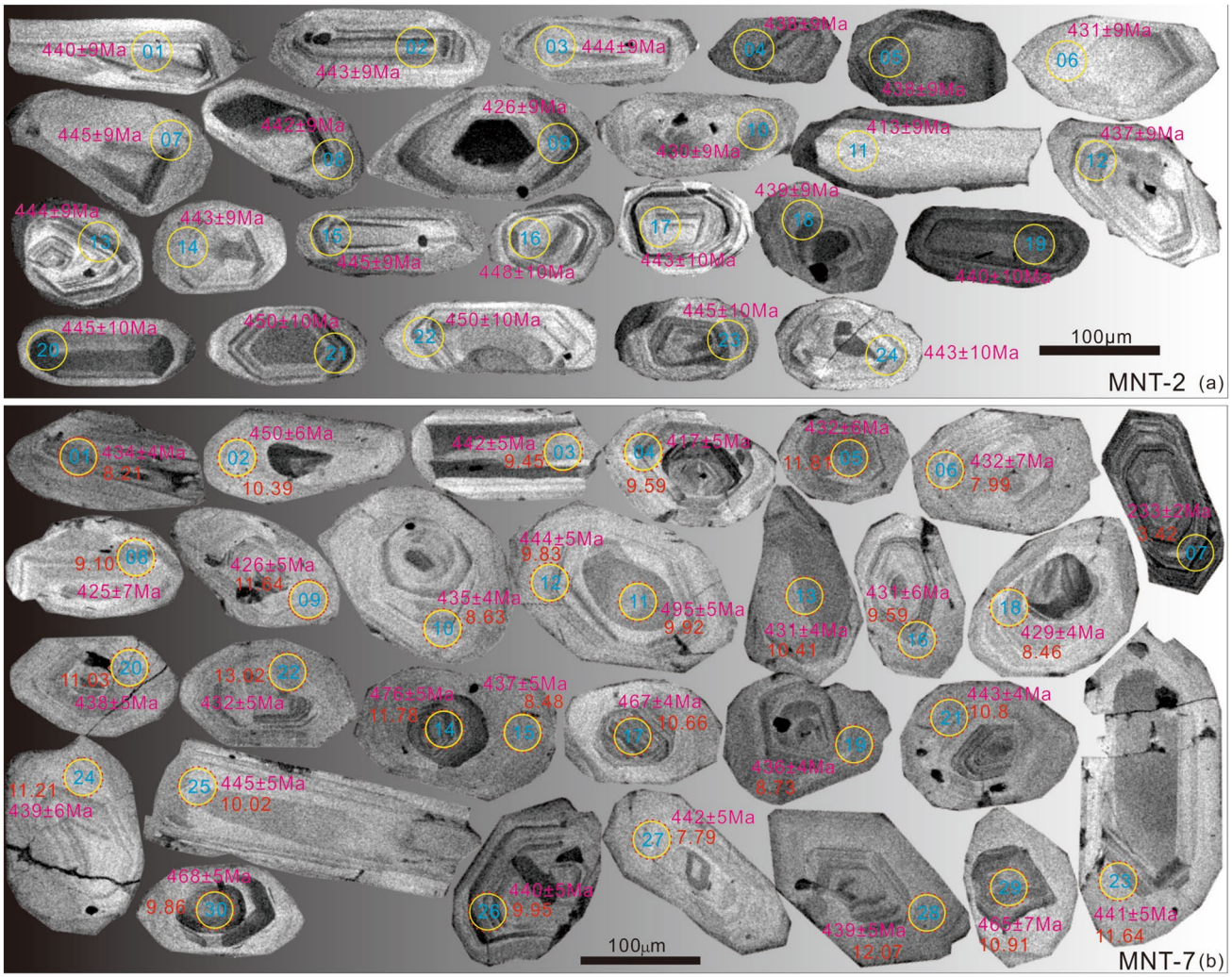

Fig. 4 Cathodoluminescence (CL) images of representative zircon grains from the Mengkete quartz diorite in the BTMB, southern margin of the EKOB. **a** Sample MNT–02; **b** sample MNT–07. The yellow solid and red dashed circles show the locations for U-Pb and Lu-Hf isotope analysis, respectively. Their corresponding $^{206}Pb/^{238}U$ ages (yellow digits) and εHf(t) values (red digits) are also shown

The trace-element results for the Mengkete quartz diorites indicate low REE contents (47.61–163.08 ppm with an average of 87.53 ppm), fractionation between LREEs and HREEs (LREE/HREE = 3.58–11.53 with an average of 7.08), and enrichment in LREEs with depletion in HREEs (Fig. 8a). All of the diorites have weakly positive Eu anomalies (Eu/Eu* = 0.96–1.32) (Fig. 8a). LREE fractionation is also indicated by the $(La/Sm)_N$ values (1.20–5.65 with an average of 3.20). The HREE depleted is probably caused by the residual garnet and hornblende (Patino-Douce and Johnston 1991), which have La/Yb ratios ranging from 3.37 to 20.98 (average: 11.41), $(La/Yb)_N$ ratios ranging from 2.42 to 15.05 (average: 8.19), and $(Gd/Yb)_N$ ratios ranging from 1.42 to 2.00 (average: 1.64).

The Mengkete quartz diorites are characterized by high Sr, low Y, and low Yb, with Rb/Sr ratios of 0.05–0.09, Ra/Ba ratios of 0.05–0.11, and high K/Rb ratios (118.98–143.23). A primitive mantle-normalized spidergram (Fig. 8b) indicates that the diorites are enriched in LILEs (such as Rb, Th, and Ba) and depleted in HFSEs (such as Nb, Ta, Zr, Hf, and Ti). The relatively enriched Zr and depleted Nb, Ta, and Ti indicate that a crustal rock is a possible source of hese diorites (Green et al.1987; Green 1995; Barth et al. 2000). The curves of the spidergrams and the REE patterns are identical across all samples, which is indicative of their cognate source rock.

Zircon *in-situ* Lu-Hf isotopic compositions

To determine the magma source for the Mengkete quartz diorite, the Lu-Hf isotopic compositions of a set of representative zircon samples (MNT-07, ~ 435.9 Ma) were

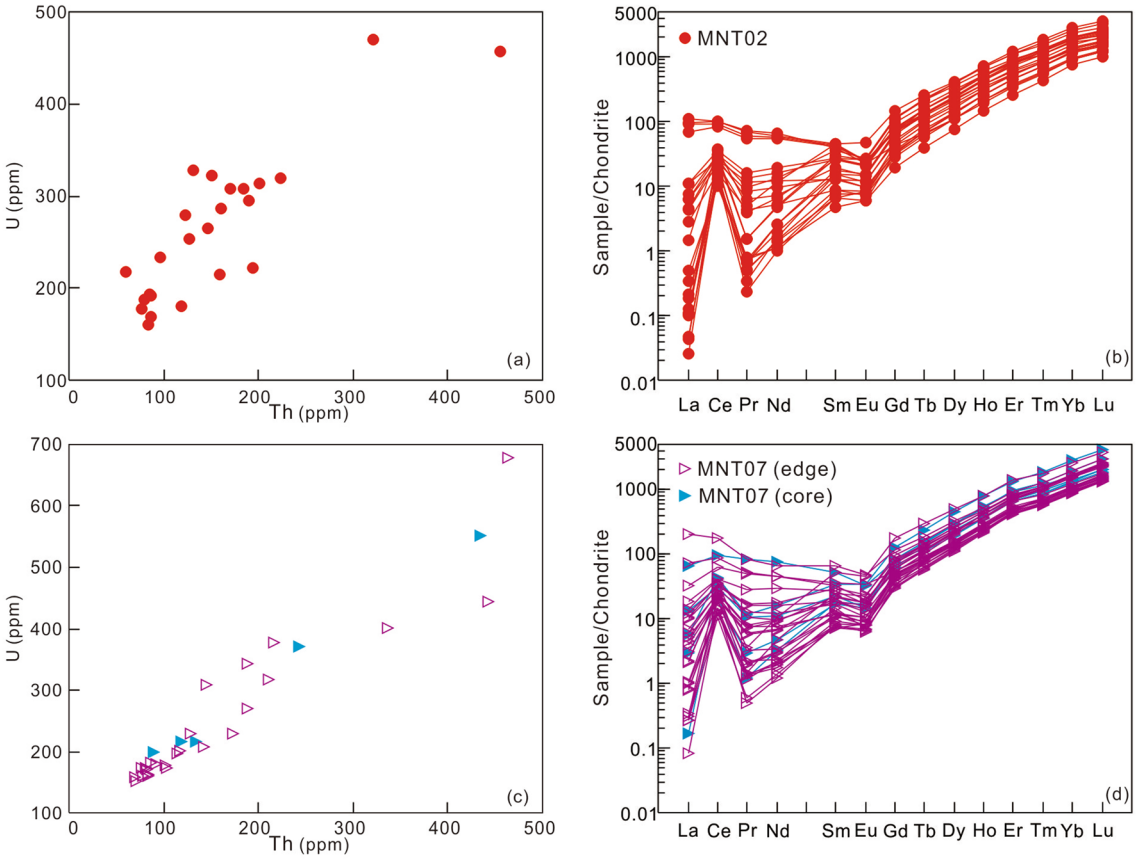

Fig. 5 Th–U contentand and chondrite-normalized REE patterns for zircon grains from Mengkete quartz diorite in the BTMB, southern margin of the EKOB (chondrite data data for normalization taken from Sun and McDonnough 1989) (**a** and **b**, sample MNT–02; **c** and **d**, sample MNT–07)

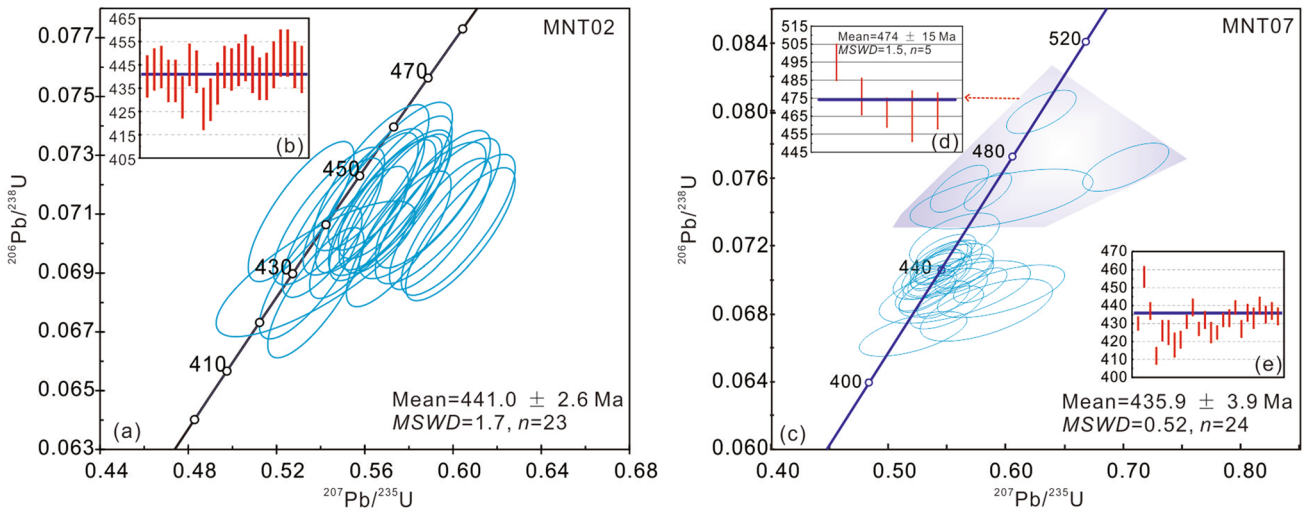

Fig. 6 LA–ICP–MS zircon U–Pb concordia diagram of the Mengkete quartz diorite in the BTMB, southern margin of the EKOB (**a** and **b**, sample MNT–02; **c**, **d** and **e**, sample MNT–07)

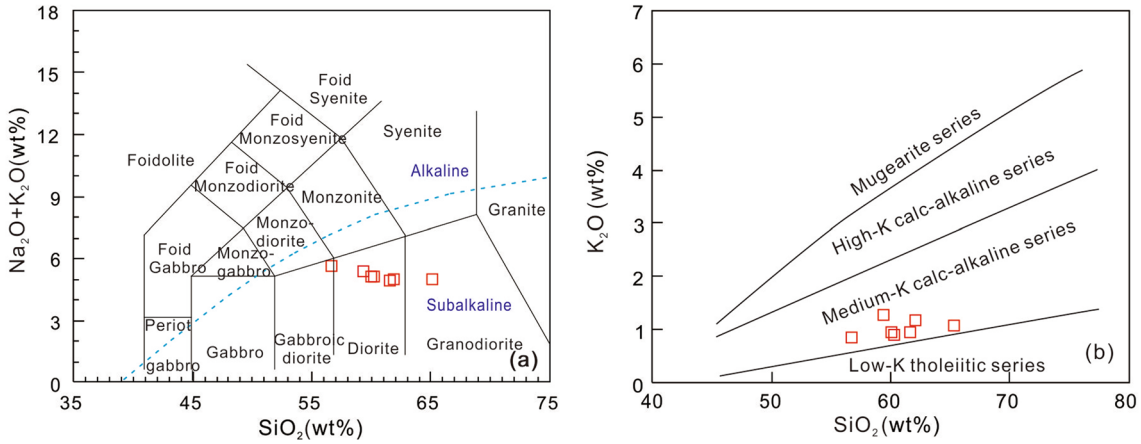

Fig. 7 **a** TAS diagrams (after Le Maitre 2002 Middlemost 1994). **b** K_2O–SiO_2 diagrams (after Rickwood 1989) of the Mengkete quartz diorite in the BTMB, southern margin of the EKOB

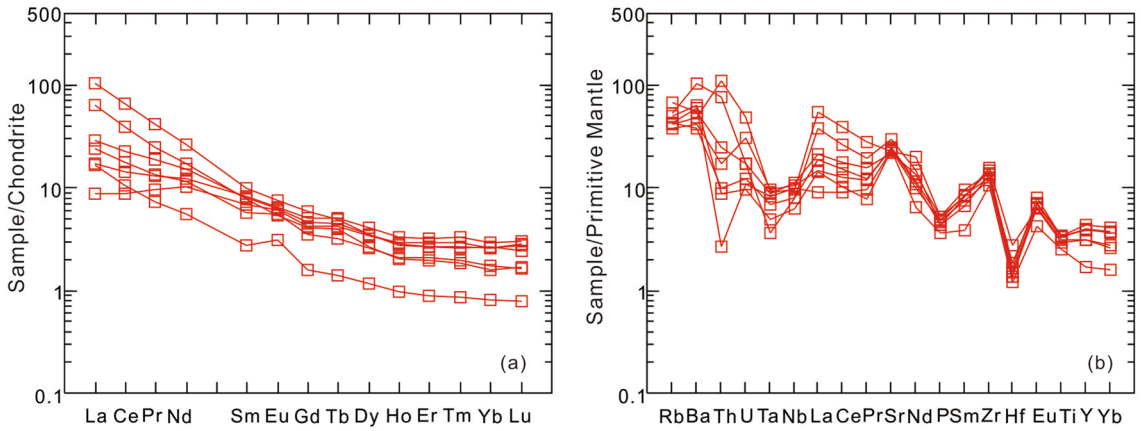

Fig. 8 **a** Chondrite-normalized rare earth element (REE) patterns, **b** primitive mantle-normalized incompatible element distribution patterns for Mengkete quartz diorite in the BTMB, southern margin of the EKOB (chondrite data and primitive mantle data for normalization taken from Sun and McDonnough 1989)

analyzed. The beam positions are shown in Fig. 4b, and the analytical results are listed in Table S4.The $^{176}Yb/^{177}Hf$ ratios of the samples range from 0.018122 to 0.066622. The $^{176}Lu/^{177}Hf$ ratios are smaller than 0.002 (range: 0.000598–0.001919), indicating that only a small amount of radiogenic Hf accumulated after the zircons crystallized (Griffin et al. 2000). Therefore, the initial $^{176}Hf/^{177}Hf$ ratio can also be used to represent the final $^{176}Hf/^{177}Hf$ ratio—that is, the ratio when the zircons initially formed (Wu et al. 2007). The $f_{Lu/Hf}$ values ranged from -0.94 to -0.98 (average: -0.97). The *in-situ* Lu-Hf isotopic compositions of the zircons in the Mengkete quartz diorites are homogenous and have similar ε_{Hf} (t) values (7.79–13.02) (Fig. 9a) and T_{DM2} model ages (1130–657Ma) (Fig. 9b).

Discussion

Petrogenesis and source characteristics

The Mengkete quartz diorites have La/Nb ratios greater than 1.0 (range 1.33–5.53). These are different from the values that mantle-derived magma would have (DePaolo and Daley 2000), indicating that these quartz diorites formed in crust-derived magma. The depleted Nb, Ta and Ti also indicate that the source was dominated by crustal materials. The Rb/Sr ratios range from 0.05 to 0.09 (average: 0.06, closer to the average crustal value of 0.24, Taylor and McLennan 1985), again supporting the hypothesis that the quartz diorites are associated with crust-derived magma.

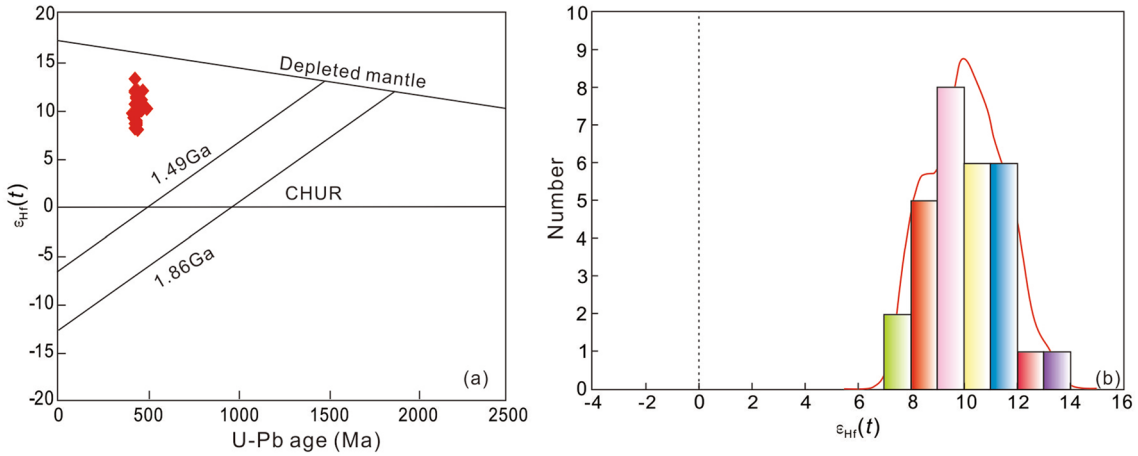

Fig. 9 **a** Plot of ε_{Hf} (t) vs. U-Pb ages and **b** Histogram of εHf (t) for zircons from studied diorite (the values used for constructing the depleted mantle and crust reference evolution lines are after Griffin et al. 2000, 2002)

The magma derived from the partial melting of basaltic rocks in the crust can form a basaltic and metaluminous granitic magma (Wolf and Wyllie 1989; Beard and Lofgren 1991; Johannes et al. 2003; Sisson et al. 2005). The high K/Rb, high Sr/Y, low Rb/Sr, and low Rb/Ba ratios obtained for the diorites indicate that the source rocks were depleted in Rb and enriched in Sr and Ba, whereas the low Rb/Sr and Rb/Ba ratios and high $Mg^{\#}$ values indicate that the source rocks consisted of mafic rocks, metabasalt, or mafic metagreywackes (Altherr et al. 2000; Liegeois 1998). In a plot of $Al_2O_3/(MgO + FeO_{Total})$ vs $CaO/(MgO + FeO_{Total})$ (an AMF-CMF diagram) (Fig. 10a), all of the samples plot in the field that corresponds to the melting of basaltic rocks. In an SiO_2–$Mg^{\#}$ diagram (Fig. 10b), all of the samples plot in or lie close to the field corresponding to adakite melts, also indicating a mafic source rock. According to plots of La/Sm vs La and Zr/Sm vs Zr plots (Fig. 10c, d, respectively), all of the samples were affected by partial melting during the evolution of the magma. This is also supported by the slightly positive Eu anomalies and LREE-HREE fractionation (Fig. 8a), which both indicate that the Mengkete quartz diorites were formed by partial melting of mafic crustal rock.

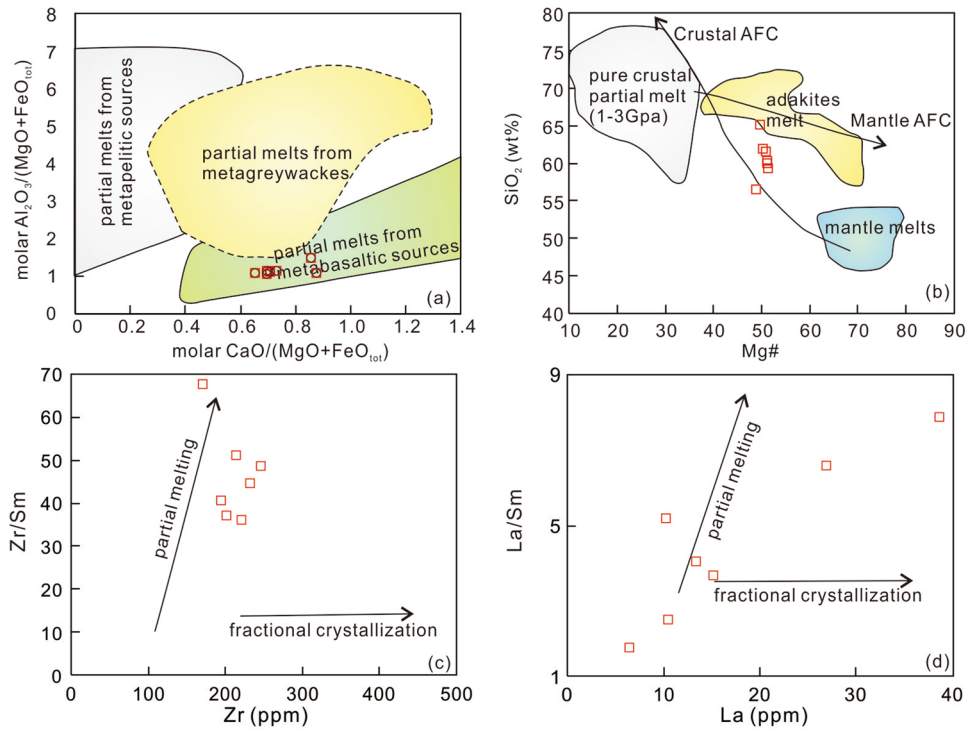

Fig. 10 **a** AMF–CMF diagram (after Sylvester 1998); **b** SiO_2–Mg# diagram (the curves of mantle assimilation–fractional crystallization (AFC) and crustal AFC are after Stern and Kilian 1996); **c** Zr/Sm–Zr diagram; **d** La/Sm–La diagram (after Allègre and Minster 1978) for Mengkete quartz diorite in the BTMB, southern margin of the EKOB

Zircon Hf isotope analysis is an important means of determining the source area for granite (Wu et al. 2007). We found that $\varepsilon_{Hf}(t)$ for zircons from the Mengkete quartz diorites was dominated by positive values ranging from +7.79 to +13.02 (Fig. 9a), with corresponding T_{DM2} model ages ranging from 1130 to 657 Ma. In the $\varepsilon_{Hf}(t)$-t diagram, all of the samples plot above the chondritic uniform-reservoir evolution line and below the depleted-mantle evolution line, indicating that the petrogenesis involves young components. There are two possible ways for young components to participate in the petrogenesis of granite. One way involves the mixture of the felsic magma formed by the partial melting of the mantle source with the lower crustal material (Griffin et al. 2002; Belousova et al. 2006; Kemp et al. 2007); in the other, mantle-derived magma underplating causes partial melting of the crustal material (Jahn et al. 2000; Wu et al. 2006; Zheng et a1. 2007). Values of $\varepsilon_{Hf}(t)$ for the Mengkete quartz diorite are positive and do not vary by more than 6 ε units. The Hf isotope values are relatively uniform, possibly indicating partial melting of the crustal material to form granitic magma. These values are also consistent with the geochemical characteristics of control by a crustal source.

The $^{176}Lu/^{177}Hf$ value for sample MNT-7 was less than 0.002, indicating that only a small amount of radiogenic Hf in the zircon after it formed. The sample had an average $f_{Lu/Hf}$ value of − 0.97, which is much lower than that of both mafic crust (− 0.34; Amelin et al., 2000) and salic crust (− 0.72; Vervoort et al., 1996). Therefore, the two-stage model age better represents the time when the source rock material was extracted from the depleted mantle (Wu et al. 2007). According to the two-stage granite model age, the Mengkete quartz diorite formed by partial melting of the Meso-Neoproterozoic crustal material.

Tectonic setting

The Mengkete quartz diorites have an SiO_2 content of 56.63–65.22%, an MgO content of 2.12–3.23%, a high Sr content (467.89–626.53 ppm), a low Y content (7.79 20.10 ppm), and a low Yb content (0.80–2.03 ppm), all of which suggest an association with adakite (Default and Drummond 1990; Martin 1999). The high Na_2O content (3.81–4.77%), low K_2O/Na_2O ratios (0.17–0.31), high Mg# values (48.92–51.29), slightly positive Eu anomalies, and in some cases high Sr/Y ratios (26.14–63.78) differ from what would be observed for typical crust-derived calc-alkaline granite (Defant and Drmmond 1990; Martin 1999). Altogether, these geochemical signatures; the high Sr, low Y, and low Yb; the Rb/Sr ratios (0.05–0.09), Rb/Ba ratios (0.05–0.11), and high K/Rb ratios (118.98–143.23); the negative Nb, P, and Ti anomalies; and the positive Sr anomalies indicate an affinity with a mafic-magma source in a subduction-related arc environment (Pearce and Norry 1979; McCulloch and Gamble 1991). The relatively enriched Ba and Sr and the relatively depleted Rb, Nb, Ta, P, and Ti also support the idea of an arc-magma source (Fig. 7b).

These results for the Mengkete quartz diorites and those from previous research on coeval magmatic rocks in the Buqingshan area—including the Bairiqiete and Yikehalaer granodiorites and intermediate-to-acidic lava—plot in the volcanic-arc granitoid (VAG) field in a Rb vs (Yb + Ta) diagram (Fig. 11a), thus further supporting an arc environment origin for the diorites. In a diagram of Rb vs (Y + Nb) (Fig. 11b), most of the data fall into the VAG and post-collision granites fields, indicating that these intermediate-to-acidic igneous rocks all formed in the same setting (Liu 2011; Li et al. 2014b). Thus, it can be concluded that the Mengkete quartz diorites are products of Early Paleozoic

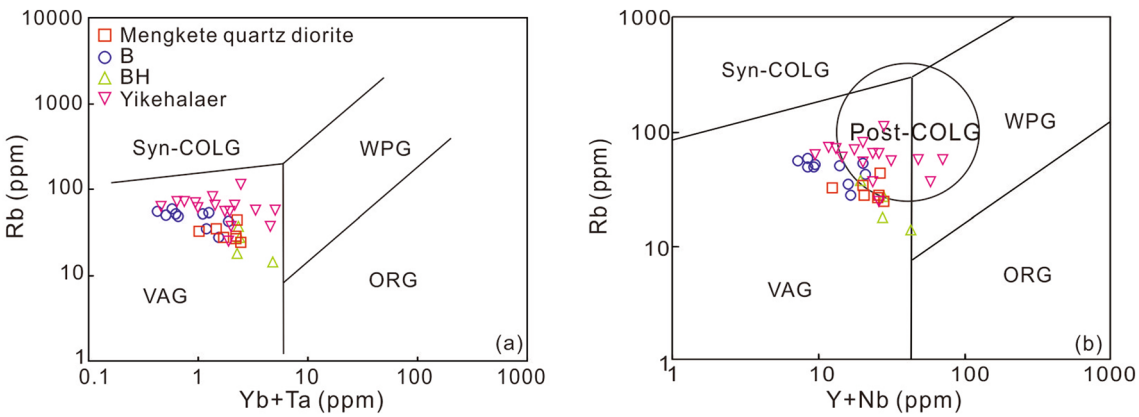

Fig. 11 Tectonic setting discrimination diagrams for Mengkete quartz diorite in the BTMB, southern margin of the EKOB (**a**, after Pearce et al. 1984; **b** after Pearce 1996). Mengkete quartz diorite data from this paper; B–Bairiqiete granodiorite data from Li et al. 2014b; BH–Bairiqiete intermediate–acid Lava data from Liu et al. 2011c; Yikehalaer–Yikehalaer granodiorite data from Li et al. 2015. *ORG,* Ocean Ridge Granites; *Post–COLG*, Post-Collision Granites; *Syn–COLG*, Syn-Collision Granites; *VAG,* Volcanic Arc Granites; *WPG* Within Plate Granites

island-arc magmatism related to Proto-Tethyan subduction and orogenesis.

Tectonic significance

The Mengkete quartz diorites (rock mass) formed between 441.0 ± 2.6 Ma and 435.9 ± 3.9 Ma and are products of Early Paleozoic island-arc magmatism related to Proto-Tethyan subduction and orogenesis. The Mengkete quartz diorites are in fault contact with the surrounding pre-Tiassic strata. All of this indicates that the Buqingshan area had a complex tectonic evolutionary history and experienced a series of tectonic events. The different stages of this history are described in detail below.

Stage 1: the beginning of the Neoproterozoic to 516 Ma (Fig. 12a). At present, the Early Paleozoic ophiolites in the BTMB are represented by Delisitan ORB ophiolites (DO, gabbro age is 516.4 ± 6.3Ma–467.2 ± 0.9Ma, Bian et al. 1999a; Liu et al. 2011a, abbreviations explained in Fig. 12), A'nyemaqen Majixueshan ORB ophiolite (gabbro 535 ± 10Ma, Li et al. 2007), and Kuhai oceanic island gabbro (555 ± 9Ma, Li et al. 2007). This is evidence that the Proto-Tethyan Ocean opened in the Early Cambrian. The Early Paleozoic ophiolite in the Buqingshan area is likely to be related to the break-up of the Rodinia supercontinent during late Neoproterozoic to Early Cambrian. This shows that in the Early Paleozoic, the East Kunlun Block, West Qinling Block, and Bayan Hara Block were in a discrete from each other and the southern margin of the East Kunlun was been an open "Buqingshan paleo-ocean basin" (Fig. 12a, Li et al. 2007; Feng et al. 2010; Liu et al. 2011a, b, c; Pei et al. 2018; Yu et al. 2020). A contemporaneous ophiolite was also found in the East Kunlun area, indicating that the Central of East Kunlun Ocean was also opened (e.g., Qingshuiquan ophiolite, 522.3 Ma–507.7 Ma, Yang et al. 1996; Chen et al. 2008; Qingshuiquan-Tatuo ophiolites, 516 Ma–485 Ma, Li et al. 2021; Qushi'ang Ophiolite, 505 Ma–498 Ma, Li et al. 2019b; Kekesha-Kekekete mafic-ultramafic melange belt, 509.4 ± 6.8 Ma, Feng et al. 2010). In addition, the Late Sinian Dundeshaerguole Pluton (DP, 544.8 ± 7.8 Ma, Li et al. 2018a, Fig. 12a) of the Kekesha area also exhibits evidence of the extension-related magmatic events that occurred in the East Kunlun area.

Stage 2: from 516 to 441 Ma (Fig. 12b). As the Buqingshan paleo-ocean basin continued to expand, the Buqingshan ocean basin began to subduct toward the north in the Late Cambrian. The Late Cambrian–Early Ordovician Manite island-arc granite (Fig. 12b, MNP, 487–479 Ma, Li et al. 2017), Deerni island-arc diorite (493 ± 6Ma, Li et al. 2007) formed in the BTMB at this time. At the same time, the intermediate-acid arc igneous complex formed in the north of the Qingshuiquan–Kekesha–Kekekete area in the East Kunlun area (KP, 515 Ma–527 Ma, Zhu et al. 2002; Zhang et al. 2010a; Zhang 2010).

Stage 3: from 441 to 400 Ma (Fig. 12c). Further subduction within the Silurian Buqingshan–A'nyemaqen Ocean led to the formation of an island-arc magma represented by the Mengkete quartz diorite (441–436 Ma), the Yikehalaer arc granodiorite (YP, 437–402 Ma, Bian et al. 2007; Liu 2011), the Bairiqiete island-arc pluton (BP, 441–439 Ma, Liu 2011, Li et al. 2014b), and the intermediate-to-acidic lava (BV, 437 Ma, Liu et al. 2011c). These island-arc-type magmatic rocks indicate that the Buqingshan–A'nyemaqen Ocean slab continued to subduct northward from the Early Cambrian to the Late Silurian. However, there was little development of the Late Paleozoic magmatic rocks in the Buqingshan and East Kunlun areas (Pei et al. 2018), suggesting that the Late Silurian Buqingshan–A'nyemaqen oceanic ridge spreading activity may have waned and that the oceanic crustal subduction activities may also have waned or stopped. By contrast, the East Kunlun area was affected by the Caledonian orogeny, and the Central of East Kunlun Ocean Basin was closed in the Late Silurian. At this point, the NEKB and SEKB collided (Chen et al. 2002b, 2007; Yin and Zhang 2003; Li et al. 2013b; Pei et al. 2018), which led to the Central of East Kunlun ophiolites thrust in place, accompanied by strong deformation and metamorphism (Meng et al. 2017, Fig. 12c). During the period 425–400 Ma, post-collision plutons, A-type granites, and Maoniushan molasse assemblage in the EKOB were formed (Liu et al. 2012; Xu et al. 2007; Lu et al. 2010; Zhang et al. 2010b; Li et al. 2013a; Chen et al. 2020; Dong et al. 2020; Li et al. 2020; Wang et al. 2022). Most researchers consider that when the Early Paleozoic oceanic basin was closed, the stress regime in the north–south direction transformed from compression to extension. This represented the end of the Early Paleozoic Proto-Tethyan evolution and the beginning of Late Paleozoic Paleo-Tethyan evolution (Yang et al. 2004; Ren 2004; Zhu et al. 2006; Mo et al. 2007; Chen et al. 2007, 2008; Mo 2010; Li et al. 2012; Xiong et al. 2014).

Stage 4: from 400 to 240 Ma (Fig. 12d). Carboniferous island/seamount basalt–limestone assemblages are present in the BTMB. The eastern Haerguole ophiolite (332 Ma) is present in the BTMB along with the Deerni ophiolite (308–345Ma) in the A'nyemaqen area (Chen et al. 2001; Yang et al. 2004, 2005). The presence of these ophiolites indicates that the Buqingshan–A'nyemaqen Ocean still existed in the Early Carboniferous. In the Late Permian, the Buqingshan–A'nyemaqen ocean once again began to subduct under the East Kunlun Block (Yang et al. 2005). Between 240 and 260 Ma, continental margin arc-type plutons (CMAP) caused by the subduction of oceanic crust is distributed in an east–west direction in the East Kunlun area (e.g., Liu et al. 2004; Yang et al. 2005; Sun et al. 2009; Li et al. 2018c; Ma et al. 2015; Chen et al. 2017; Zhao et al.

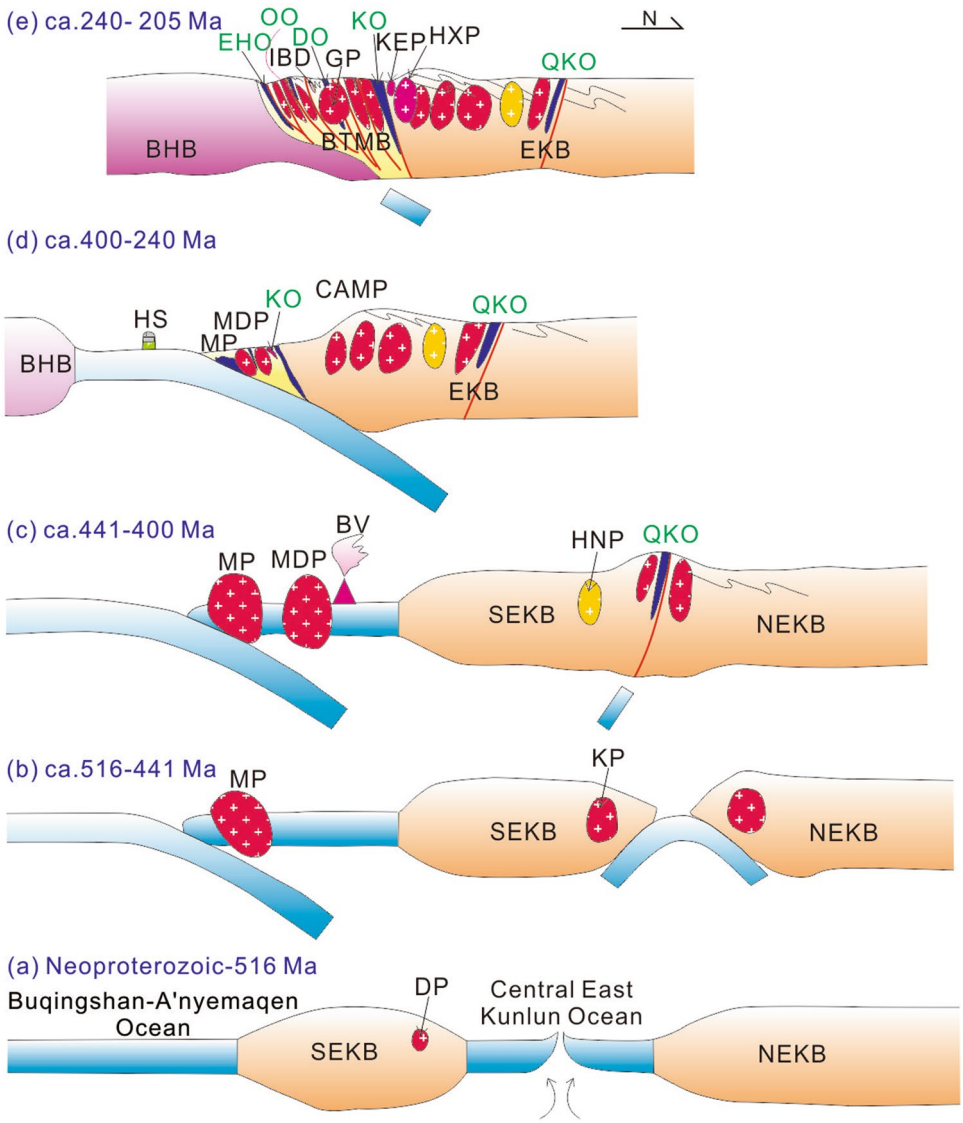

Fig. 12 Tectonic evolution cartoon of Buqingshan–A'nyemaqen Ocean in Paleozoic–Early Mesozoic (modified from Pei et al. 2018) in the southern margin of the EKOB. *SEKB*, Southern East Kunlun Block; *NEKB*, Northern East Kunlun Block; *CEKB*, Central East Kunlun Belt; *BHB*, Bayan Har Block; *BTMB*, Buqingshan–A'nyemaqen Tectonic mélange belt; *QKO*, Qingshuiquan-Kekesha Ophiolite, 522–509 Ma, after Lu et al. (2002), Yang et al. (1996), Feng et al. (2010), Li et al. (2013b). DO-Delisitan Ophiolite, 516.4 Ma, after Liu et al. (2011c); KO-Kekekete Ophiolite, 501 Ma, Li et al. (2013b); OO-Ordovician Ophiolite, 467–450 Ma, after Pei et al. unpublish; EHO-Eastern Haerguole Ophiolite, 332.8 Ma, after Liu et al. (2011c); DP-Dundeshaerguole Plutons, 544.8 Ma, Li et al. (2018a); KP-Kekesha Pluton, 515.2 Ma, after Zhang et al. (2010a); MP-Manite Plutons, 487–479 Ma, after Li et al. (2017); BV-Bairiqiete volcanic, 437.7 Ma, after Liu et al. (2011a); MDP-Mengkete Pluton, 441.0~435.9 Ma, this paper; HNP-Helegang Naren Pluton, 425.0 Ma, after Li et al. (2013a), A-type granite; HS-Haerguole Seamount Basalt age 340.8 Ma, after Yang et al. (2014); CMAP-Late Permian-Middle Triassic Continental margin arc type Plutons, 260–240 Ma, Liu et al. (2004), Liu (2008), Yang et al. (2005), Sun et al. (2009), Ma et al. (2015), Chen et al. (2017), Xiong et al. (2015), Li et al. (2018b). HXP-Helegang Xilikete Pluton, 225 Ma, after Chen et al. (2013a); GP-Gerizhuotuo Pluton, 225.8–224 Ma, after Li et al. (2013c); Liu et al. (2015); KEP-Kekeealong Plutons, 218.3 Ma, Chen et al. (2013b); IBD-intermediate-basic dikes, 205 Ma, after Li et al. (2019a)

2019; Kong et al. 2020; Yu et al. 2020; Zhou et al. 2020; Li et al. 2022 Fig. 12d). This stage is akin to Andean continental margin subduction.

Stage 5: from 240 to 205 Ma (Fig. 12e). The Gerizhuotuo diorite with attribute of "stitching pluton" was found in the Buqingshan area (GP, 225–224 Ma, Li et al. 2013c; Liu et al. 2015). The Kekeealong Pluton and Helegang-Xilikete Pluton in the SEKB (KP, Chen et al. 2013a; HXP, Chen et al. 2013b), the Elashan Formation rhyolite, which is high in Nb and Ta, and the gabbro representative of the post-collision extension magmatic rock (Luo et al. 2002; Ding et al. 2011) indicate that the 225 Ma Buqingshan–A'nyemaqen Ocean

had closed by this time. The late Late Triassic massive intermediate-basic dikes represent the latest tectonic magmatism in the BTMB (IBD, 205Ma, Li et al. 2019a). During this period, an orogenic collision event finally formed a series of NNE−SSW striking thrust faults (Fig. 2), and tectonic blocks of different ages and genesis mixed with the Maerzheng Formation flysch turbidite, thus forming the basic tectonic framework of the Buqinshan–A'nyemaqen complex accretive type tectonic mélange belt (Fig. 12e). At the same time, the entire EKOB and main structural framework of the Central Orogenic Belt of China were created (Pei et al. 2018). Therefore, it can be seen that the BTMB at the southern margin of the EKOB records the long-lived history of the subduction and accretion that occurred during the Late Neoproterozoic, Paleozoic, and Early Mesozoic, as well as the final closure of the Buqingshan–A'nyemaqen Ocean in the late Middle Triassic. It also records the evolution of the Proto-Tethys Ocean and Paleo-Tethys Ocean at the southern margin of the EKOB.

Conclusion

From a comprehensive study of the Mengkete quartz diorites in the BTMB based on geochronological, geochemical, and zircon Hf isotopes data, we conclude the following

1. The LA-ICP-MS zircon ages of the Mengkete quartz diorites (rock mass) are between 441.0 ± 2.6 Ma and 435.9 ± 3.9 Ma), indicating that the intrusion formed in the Early Silurian.
2. The Mengkete quartz diorites have high Al_2O_3, low alkali, and medium K_2O contents and belong to the medium-K calc-alkaline series. The zircon Hf isotope compositions gave a T_{DM2} model age range of 1130–657 Ma, indicating that the diorites are derived from the partial melting of mafic rocks in the Meso-Neoproterozoic lower continental crust.
3. The BTMB in the southern margin of the EKOB had a long-lived subduction and accretion history during the Late Neoproterozoic, Paleozoic, Early Mesozoic and finally closed in the late Middle Triassic. The evolution of both the Proto-Tethyan Ocean and the Paleo-Tethyan Ocean is recorded here.

Supplementary Information The online version contains supplementary material available at https://doi.org/10.1007/s00531-022-02223-z.

Acknowledgments We wish to acknowledge Dr. Liu Xiaoming and Dr. Diwu Chunrong, at the Northwest University, State Key Laboratory of Continental Dynamics, for assistance with LA-ICP-MS dating; and Li He at the Institute of Geology and Geophysics, State Key Laboratory of Lithosphere Evolution, for assistance with conducting XRF and trace element analyses. This manuscript has been greatly improved by critical reviews by three anonymous reviewers and the editor in chief Ulrich Riller, associate editor Soumyajit Mukherjee. The authors would like to thank Enago (www.enago.cn) for the English language review. This study was supported financially by the National Nature Sciences Foundation of China (Nos. 41872235, 42172236, 41872233, 42072254, 42102260, 42072267, 42072261, 41902046, 41802234, 41602229), China Scholarship Council (No. 201806565026), the Commonweal Geological Survey, the Aluminum Corporation of China and the Land-Resources Department of Qinghai Province (Grant No. 200801), China Geological Survey (Nos.12120114041201, DD2016007901), Natural Science Basic Research Plan in Shaanxi Province of China (Grants Nos. 2019JM-312, 2019JQ-090, 2019JQ-209, 2018JM4017), China Postdoctoral Science Foundation (No. 2016M592726), and the Fundamental Research Funds for the Central Universities (Nos. 300102270202, 202110710062, 300103183081, 300104282717, 300102279204, and 201810710233).

References

Allègre CJ, Minster JF (1978) Quantitative models of trace element behavior in magmatic processes. Earth Planet Sci Lett 38(1):1–25. https://doi.org/10.1016/0012-821X(78)90123-1

Altherr R, Holl A, Hegner E, Langer C, Kreuzer H (2000) High-potassium, calc-alkaline I-type plutonism in the European variscides: northern vosges (France) and northern Schwarzwald (Germany). Lithos 50(1–3):51–73. https://doi.org/10.1016/S0024-4937(99)00052-3

Amelin Y, Lee DC, Halliday AN (2000) Early-middle Archean crustal evolution deduced from Lu-Hf and U-Pb isotopic studies of single zircon grains. Geochim et Cosmochim Acta 64(24):4205–4235. https://doi.org/10.1016/S0016-7037(00)00493-2

Andersen T (2002) Correlation of common lead in U-Pb analyses that do not report ^{204}Pb. Chem Geol 192(1–2):59–79. https://doi.org/10.1016/S0009-2541(02)00195-X

Barth MG, McDonough WF, Rudnick RL (2000) Tracking the budget of Nb and Ta in the continental crust. Chem Geol 165(3–4):197–213. https://doi.org/10.1016/S0009-2541(99)00173-4

Beard JS, Lofgren GE (1991) Dehydration melting and water-saturated melting of basaltic and andesitic greenstones and amphibolites at 1.3 and 6.9 kb. J Petrol 32(2): 365–401. https://doi.org/10.1093/petrology/32.2.365

Belousova EA, Griffin WL, O'Reilly SY, Fisher NI (2002) Igneous zircon: Trace element composition as an indicator of source rock type. Contrib to Mineral Petrol 143:602–622. https://doi.org/10.1007/s00410-002-0364-7

Belousova EA, Griffin WL, O'reilly SY (2006) Zircon crystal morphology, trace element signatures and Hf isotope composition as a tool for petrogenetic modelling: examples from eastern Australian granitoids. J Petrol 47(2):329–353. https://doi.org/10.1093/petrology/egi077

Bian QT, Chang CF, Zheng XS (1997) Basic geotectonic characteristics of the Hoh Xil region of Qinghai province, China. Sci Geol Sin 32:37–46 ((**in Chinese with English abstract**))

Bian QT, Luo XQ, Chen HH, Zhao DS, Li DH (1999a) Zircon U-Pb age of granodiorite-tonalite in the A'nyemaqen ophiolitic belt and its tectonic significance. Sci Geol Sin 34:420–426 ((**in Chinese with English abstract**))

Bian QT, Luo XQ, Li HS, Chen HH, Zhao DS, Li DH (1999b) Discovery of early paleozoic and early carboniferous-early permian ophiolites in the A'nymaqen, Qinghai province, China. Sci Geol Sin 34:523–524 ((**in Chinese**))

Bian QT, Yin LM, Sun SF, Luo XQ, Pospelov I, Astrakhahtsev O, Chamov N (2001) Discovery of Ordovician acritarchs in

Buqingshan ophiolite complex, East Kunlun mountains and its significance. Chin Sci Bull 46:341–345. https://doi.org/10.1007/BF03187200

Bian QT, Li DH, Pospelov I, Yin LM, Li HS, Zhao DS, Chang CF, Luo XQ, Gao SL, Astrakhantsev O, Chamov N (2004) Age, geochemistry and tectonic setting of Buqingshan ophiolites, north Qinghai-Tibet Plateau China. J Asian Earth Sci 23(4):577–596. https://doi.org/10.1016/j.jseaes.2003.09.003

Bian QT, Pospelov II, Li HM, Chang CF, Li JL (2007) Discovery of the end-early Paleozoic adakite in the Buqingshan area, Qinghai province, and its tectonic implications. Acta Petrol Sin 23: 925–934 **(in Chinese with English abstract)**. https://doi.org/10.1631/jzus.2007.B0900

Bouvier A, Vervoort JD, Patchett PJ (2008) The Lu-Hf and Sm-Nd isotopic composition of CHUR: constraints from unequilibrated chondrites and implications for the bulk composition of terrestrial planets. Earth Planet Sci Lett 273(1–2):48–57. https://doi.org/10.1016/j.epsl.2008.06.010

Burchfiel BC, Molnar P, Zhao ZY, Liang KY, Wang SJ, Huang MM, Sutter J (1989) Geology of the Ulugh Muztagh area, northern Tibet. Earth Planet Sci Lett 94(S1–2):57–70. https://doi.org/10.1016/0012-821X(89)90083-6

Chen L, Sun Y (1999) Derni ophoplite: northrnmost Tethyan lithosphere relics in Tibet Plateau. J Northwest Uni (Nat Sci Ed) 29:141–144 ((**in Chinese with English abstract**))

Chen FK, Hegner E, Todt W (2000) Zircon ages, Nd isotopic and chemical compositions of orthogneisses from the Black Forest, Germany: evidence for a Cambrian magmatic arc. Int J Earth Sci 88(4):791–802. https://doi.org/10.1007/s005310050306

Chen L, Sun Y, Pei XZ, Gao M, Feng T, Zhang ZQ, Chen W (2001) Northernmost Paleo-Tethyan oceanic basin in Tibet: geochronol ogical evidence from $^{40}Ar/^{39}Ar$ age dating of Dur'ngoi ophiolite. Chin Sci Bull 46:1203–1205. https://doi.org/10.1007/BF02900603

Chen FK, Siebel W, Satir M, Terzioglu MN, Saka K (2002a) Geochronology of the Karadere basement (NW Turkey) and implications for the geological evolution of the Istanbul zone. Int J Earth Sci 91:469–481. https://doi.org/10.1007/s00531-001-0239-6

Chen NS, Sun M, He L, Zhang KX, Wang GC (2002b) Precise timing of the Early Paleozoic metamorphism and thrust deformation in the Eastern Kunlun Orogen. Chin Sci Bull 47:1130–1133. https://doi.org/10.1360/02tb9253

Chen L, Sun Y, Pei XZ, Feng T, Zhang GW (2004) Comparison of eastern Paleo-Tethyan ophiolites and its geodynamic significance: evidence from Dur'ngoi ophiolite. Sci China Ser D Earth Sci 47:378–384. https://doi.org/10.1360/02yd0488

Chen NS, Sun M, Wang QY, Zhao GC, Chen Q, Shu GM (2007) EMP chemical ages of monazites from central zone of the eastern Kunlun orogen: records of multi-tectonometamorphic events. Chin Sci Bull 52:2252–2263. https://doi.org/10.1007/s11434-007-0299-5

Chen NS, Sun M, Wang QY, Zhang KX, Wan YS, Chen HH (2008) U-Pb dating of zircon from the central zone of the east Kunlun orogen and its implications for tectonic evolution. Sci China Ser D Earth Sci 51:929–938. https://doi.org/10.1007/s11430-008-0072-x

Chen GC, Pei XZ, Li RB, Li ZC, Pei L, Liu ZQ, Chen YX, Liu CJ, Gao JM, Wei FH (2013a) Geochronology and genesis of the Helegang Xilikete granitic plutons from the southern margin of the eastern East Kunlun Orogenic Belt and their tectonic significance. Acta Geol Sin 87(10):1525–1541 ((**in Chinese with English abstract**))

Chen GC, Pei XZ, Li RB, Li ZC, Pei L, Liu ZQ, Chen YX, Liu CJ, Gao JM, Wei FH (2013b) Zircon U-Pb geochronology, geochemical characteristics and geological significance of Cocoe A'Long quartz diorites body from the Hongshuichuan area in East Kunlun. Acta Geol Sin 87(2):178–196 ((**in Chinese with English abstract**))

Chen GC, Pei XZ, Li RB, Li ZC, Liu CJ, Chen YX, Pei L, Zhang YM, Wang M, Li XB, Zhang Y (2017) Age and petrogenesis of jialuhe basic-intermediate pluton in xiangjiananshan granite batholith in the eastern part of east kunlun orogenic belt, and its geological significance. Geotecton et Metallog 41(6):1097–1115 ((**in Chinese with English abstract**))

Chen JJ, Fu LB, Wei JH, Selby D, Zhang DH, Zhou HZ, Zhao X, Liu Y (2020) Proto-Tethys magmatic evolution along northern Gondwana: insights from Late Silurian-Middle Devonian A-type magmatism, East Kunlun Orogen, Northern Tibetan Plateau China. Lithos 356–357:105304. https://doi.org/10.1016/j.lithos.2019.105304

De Paolo DJ, Daley EE (2000) Neodymium isotopes in basalts of the southwest basin and range and lithospheric thinning during continental extension. Chem Geol 169(1–2):157–185. https://doi.org/10.1016/S0009-2541(00)00261-8

Defant MJ, Drummond MS (1990) Derivation of some modern arc magmas by melting of young subducted lithosphere. Nature 347:662–665. https://doi.org/10.1038/347662a0

Ding S, Huang H, Niu YL, Zhao ZD, Yu XH, Mo XX (2011) Geochemistry, geochronology and petrogenesis of East Kunlun high Nb-Ta rhyolites. Acta Petrol Sin 27(12): 3603–3614 **(in Chinese with English abstract)**. https://doi.org/10.1080/00288306.2011.590212

Dong YP, He DF, Sun SS, Liu XM, Zhou XH, Zhang FF, Yang Z, Cheng B, Zhao GC, Li JH (2018) Subduction and accretionary tectonics of the East Kunlun orogen, western segment of the Central China Orogenic System. Earth Sci Rev 186:231–261. https://doi.org/10.1016/j.earscirev.2017.12.006

Feng JY, Pei XZ, Yu SL, Ding SP, Li RB, Sun Y, Zhang YF, Li ZC, Chen YX, Zhang XF, Chen GC (2010) The discovery of the mafic-ultramafic mélange in Kekesha area of Dulan county, east Kunlun region, its LA-ICP-MS zircon U-Pb age. Geol China 37(1):28–37 ((**in Chinese with English abstract**))

Green TH (1995) Significance of Nb/Ta as an indicator of geochemical processes in the crust-mantle system. Chem Geol 120(3–4):347–359. https://doi.org/10.1016/0009-2541(94)00145-X

Green TH, Pearson NJ (1987) An experimental study of Nb and Ta partitioning between Ti-rich minerals and silicate liquids at high pressure and temperature. Geochim et Cosmochim Acta 51(1):55–62. https://doi.org/10.1016/0016-7037(87)90006-8

Griffin WL, Pearson NJ, Belousova E, Jackson SE, Van Achterbergh E, O'Reilly SY, Shee SR (2000) The Hf isotope composition of cratonic mantle: LAM-MC-ICPMS analysis of zircon megacrysts in kimberlites. Geochim et Cosmochim Acta 64:133–147. https://doi.org/10.1016/S0016-7037(99)00343-9

Griffin WL, Wang X, Jackson SE, Pearson NJ, O'Reilly SY, Xu XS, Zhou XM (2002) Zircon chemistry and magma mixing, SE China: in-situ analysis of Hf isotopes, Tonglu and Pingtan igneous complexes. Lithos 61(3–4):237–269. https://doi.org/10.1016/S0024-4937(02)00082-8

Guo AL, Zhang GW, Sun YG, Cheng SY, Yao AP (2007) Geochemistry and spatial distribution of late-Paleozoic mafic volcanic rocks in the surrounding areas of the Gonghe basin: implications for Majixueshan triplejunction and east Paleotethyan archipelagic ocean. Sci China Ser D Earth Sci 50(Supp II): 292–304. https://doi.org/10.1007/s11430-007-6002-5

Iizuka T, Hirata T (2005) Improvements of precision and accuracy in in situ Hf isotope microanalysis of zircon using the laser ablation-MC-ICPMS technique. Chem Geol 220(1–2):121–137. https://doi.org/10.1016/j.chemgeo.2005.03.010

Iizuka T, Yamaguchi T, Itano K, Hibiya Y, Suzuki K (2017) What Hf isotopes in zircon tell us about crust-mantle evolution. Lithos 274–275:304–327. https://doi.org/10.1016/j.lithos.2017.01.006

Jahn BM, Wu FY, Chen B (2000) Granitoids of the Central Asian Orogenic Belt and continental growth in the Phanerozoic. Earth Environ Sci Trans R Soc Ed 91(1–2):181–193. https://doi.org/10.1017/S0263593300007367

Jiang CF, Yang JS, Feng BG, Zhu ZZ, Zhao M, Chai, YC (1992) Opening closing tectonics of Kunlun mountains. Geological Publishing House, Beijing, pp 1–217 **(in Chinese)**.

Johannes W, Ehlers C, Kriegsman LM, Mengeld K (2003) The link between migmatites and S-type granites in the Turku area, southern Finland. Lithos 68(3–4):69–90. https://doi.org/10.1016/S0024-4937(03)00032-X

Kemp AIS, Hawkesworth CJ, Foster GJ, Paterson BA, Woodhead JD, Hergt JM, Gray CM, Whitehouse MJ (2007) Magmatic and crustal differentiation history of granitic rocks from Hf-O isotopes in zircon. Science 315(5814):980–983. https://doi.org/10.1126/science.1136154

Kong JJ, Niu YL, Hu Y, Zhang Y, Shao FL (2020) Petrogenesis of the Triassic granitoids from the East Kunlun Orogenic Belt, NW China: Implications for continental crust growth from syn-collisional to post-collisional setting. Lithos 364–365:105513. https://doi.org/10.1016/j.lithos.2020.105513

Li WY, Li SG, Guo AL, Sun YG, Zhang GW (2007b) Zircon SHRIMP U-Pb ages and trace element geochemistry of the Kuhai gabbro and the Dur'ngoi diorite in the southern east Kunlun tectonic belt, Qinghai, western China and their geological implications. Sci China Ser D Earth Sci 50 (Supp II): 331–338. https://doi.org/10.1007/s11430-007-6003-4

Li RB, Pei XZ, Li ZC, Liu ZQ, Chen GC, Chen YX, Wei FH, Gao JM, Liu CJ, Pei L (2012) Geological characteristics of Late Palaeozoic-Mesozoic unconformities and their response to some significant tectonic events in eastern part of Eastern Kunlun. Earth Sci Front 19(5): 244-254 **(in Chinese with English abstract)**. https://doi.org/10.1007/s11783-011-0280-z

Li RB, Pei XZ, Li ZC, Sun Y, Pei L, Chen GC, Chen YX, Liu CJ, Wei FH (2013a) Regional tectonic transformation in east Kunlun orogenic belt in early Paleozoic: constraints from the geochronology and geochemistry of Heleganaren alkali-feldspar granite. Acta Geol Sin Engl 87(2):333–345. https://doi.org/10.1111/1755-6724.12054

Li RB, Pei XZ, Li ZC, Sun Y, Feng JY, Pei L, Chen GC, Liu CJ, Chen YX (2013b) Geochemical features, age, tectonic significance of the Kekekete mafic-ultramafic rocks, east Kunlun orogen China. Acta Geol Sin Engl 87(5):1319–1333. https://doi.org/10.1111/1755-6724.12131

Li ZC, Pei XZ, Liu ZQ, Li RB, Pei L, Chen GC, Liu CJ, Chen YX, Gao JM, Wei FH, Wu SK, Wang YC, Yang J (2013c) Geochronology and geochemistry of the Gerizhuotuo diorites from the Buqingshan tectonic mélange belt in the southern margin of East Kunlun and their geologic implications. Acta Geol Sin 87(8):1090–1103 **((in Chinese with English abstract))**

Li RB, Pei XZ, Li ZC, Pei L, Chen GC, Liu CJ, Chen YX, Liu ZQ (2014a) Geochemical characteristics of Gerizhuotuo OIB and its tectonic significance in Buqingshan tectonic mélange belt, southern margin of East Kunlun Orogen. Earth Sci Front 21(1):183–195 **((in Chinese with English abstract))**

Li ZC, Pei XZ, Li RB, Pei L, Liu CJ, Chen YX, Liu ZQ, Chen GC, Xu T, Yang J, Wei B (2014b) Geochronology, geochemistry and tectonic setting of the Bairiqiete granodiorite intrusion (rock mass) from the Buqingshan tectonic mélange belt in the southern margin of East Kunlun. Acta Geol Sin Engl 88:584–597. https://doi.org/10.1111/1755-6724.12216

Li RB, Pei XZ, Li ZC, Pei L, Liu CJ, Chen YX, Chen GC, Liu ZQ, Yang J (2015) Geochemistry and zircon U-Pb geochronology of granitic rocks in the Buqingshan tectonic mélange belt, northern Tibet Plateau, China and its implications for Prototethyan evolution. J Asian Earth Sci 105:374–389. https://doi.org/10.1016/j.jseaes.2015.02.004

Li ZC, Pei XZ, Li RB, Pei L, Liu CJ, Chen YX, Zhang YM, Wang M, Xu T (2017) Early Ordovician Island-arc type manite granodiorites pluton (rock mass) from the Buqingshan Tectonic Mélange Belt in the Southern Margin of East Kunlun: constraints on Closure of the Proto-Tethys Ocean. Geol J 52:510–528. https://doi.org/10.1002/gj.2785

Li RB, Pei XZ, Li ZC, Pei L, Chen GC, Chen YX, Liu CJ, Wang SM (2018a) Paleo-Tethys Ocean subduction in eastern section of East Kunlun Orogen: Evidence from the geochronology and geochemistry of the Wutuo pluton. Acta Petrol Sin 34(11):3399–3421 **((in Chinese with English abstract))**

Li RB, Pei XZ, Pei L, Li ZC, Chen GC, Chen YX, Liu CJ, Wang M (2018b) The Early Triassic Andean-type Halagatu granitoids pluton in the East Kunlun orogen, northern Tibet Plateau: Response to the northward subduction of the Paleo-Tethys Ocean. Gondwana Res 62:212–226. https://doi.org/10.1016/j.gr.2018.03.005

Li ZC, Li RB, Pei L, Chen YX, Liu CJ, Pei XZ, Liu ZQ, Chen GC, Li X (2018c) Magmatic response to Proto-Tethyan Ocean subduction in east section of East Kunlun: evidence from zircon U-Pb dating of late Sinian Dundeshaerguole hornblende monzonite. Earth Sci 43 (12): 4536–4550 **(in Chinese with English abstract)**. https://doi.org/10.3799/dqkx.2018c.173

Li RB, Pei XZ, Wei B, Li ZC, Pei L, Chen YX, Liu CJ, Cheng GC, Wang M, Feng K (2019a) Constraints of late Cambrian mafic rocks from the Qushi'ang ophiolite on a back-arc system in a continental margin, East Kunlun Orogen, Western China. J Asian Earth Sci 169:117–129. https://doi.org/10.1016/j.jseaes.2018.08.006

Li ZC, Pei XZ, Li RB, Pei L, Chen YX, Liu CJ, Liu ZQ, Chen GC, Wang M, Zhao SW (2019b) The latest tectonic magmatism in the Buqingshan-A'nyemaqen tectonic mélange belt: evidence from zircon U-Pb geochronology of intermediate-basic dikes, northern Tibetan Plateau, China. Arab J Geosci 12:374. https://doi.org/10.1007/s12517-019-4535-5

Li RB, Pei XZ, Li ZC, Patias D, Su ZG, Pei L, Chen GC, YX, Liu CJ (2020) Late Silurian to Early Devonian volcanics in the East Kunlun orogen, northern Tibetan Plateau: record of postcollisional magmatism related to the evolution of the Proto-Tethys Ocean. J Geodyn 140: 101780. https://doi.org/10.1016/j.jog.2020.101780

Li RB, Pei XZ, Wei B, Li ZC, Pei L, Chen GC, Chen YX, Liu CJ (2021) Middle Cambrian-Early Ordovician ophiolites in the central fault of the East Kunlun Orogen: implications for an epicontinental setting related to Proto-Tethyan Ocean subduction. Gondwana Res 94:243–258. https://doi.org/10.1016/j.gr.2021.02.017

Li ZC, Pei XZ, Bons PD, Li RB, Pei L, Chen GC, Chen YX, Liu CJ, Wang M, Zhao SW, Li XB, Gao F (2022) Petrogenesis and tectonic setting of the early-middle triassic subduction-related granite in the eastern segment of East Kunlun: evidences from petrology, geochemistry, and zircon U-Pb-Hf isotopes. Int Geol Rev 64(5):698–721. https://doi.org/10.1080/00206814.2021.1875268

Liegeois JP, Navez J, Hertogen J, Black R (1998) Contrasting origin of post-collisional high-K calc-alkaline and shoshonitic versus alkaline and peralkaline granitoids. The use of sliding normalization. Lithos 45(1–4):1–28. https://doi.org/10.1016/S0024-4937(98)00023-1

Liu CD, Mo XX, Luo ZH, Yu XH, Chen HW, Li SW, Zhao X (2004) Mixing events between the crust-and mantle-derived magmas in Eastern Kunlun: evidence from zircon SHRIMP II chronology. Chin Sci Bull 49(8):828–834. https://doi.org/10.1007/BF02889756

Liu ZQ (2011) Study on the geological characteristics and tectonic of Buqingshan mélanges belt, the south margin of east Kunlun

mountains. Chang'an University (Ph. D thesis): 1–180 **(in Chinese with English abstract)**.

Liu ZQ, Pei XZ, Li RB, Li ZC, Zhang XF, Liu ZG, Chen GC, Chen YX, Ding SP, Guo JF (2011a) LA-ICP-MS zircon U-Pb geochronology of the two suites of ophiolites at the Buqingshan area of the A'nyemaqen orogenic belt in the southern margin of east Kunlun and its tectonic implication. Acta Geol Sin 85(2):185–194 ((**in Chinese with English abstract**))

Liu ZQ, Pei XZ, Li RB, Li ZC, Chen YX, Gao JM, Liu CJ, Wang XL, Wei FH, Zhang G, Yang ZZ (2011b) Geological characteristics of the tectonic mélange belt of Buqingshan area in the southern margin of east Kunlun and its tectonic implications. Geol Bull China 30(8):1182–1195 ((**in Chinese with English abstract**))

Liu ZQ, Pei XZ, Li RB, Li ZC, Chen GC, Chen YX, Gao JM, Liu CJ, Wei FH, Wang XL, Zhang G (2011c) Early Paleozoic intermediate-acid magmatic activity in Bairiqiete area along the Buqingshan tectonic mélange belt on the southern margin of east Kunlun: constraints from zircon U-Pb dating and geochemistry. Geol China 38(5):1150–1167 ((**in Chinese with English abstract**))

Liu B, Ma CQ, Zhang JY, Xiong FH, Huang J, Jiang HA (2012) Petrogenesis of Early Devonian intrusive rocks in the east part of Eastern Kunlun Orogen and implication for early Palaeozoic orogenic processes. Acta Petrol Sin 28: 1785–1807 **(in Chinese with English abstract)**. https://doi.org/10.1021/cs300014k

Liu JL, Sun FY, Li L, Zhao FF, Wang YD, Wang S, Zhang YT (2015) Geochronology, geochemistry and Hf isotopes of Gerizhuotuo complex intrusion in west of Anyemaqen suture zone. Earth Sci 40(6): 965–981 **(in Chinese with English abstract)**. https://doi.org/10.3799/dqkx.2015.081

Lu SN, Yu HF, Zhao FQ, Jin W, Li HK, Li Q, Yang CL, Li HM, Zheng JK, Zhang MS, Jiang MM, Ge XH, Xiu QY, Zhang WZ, Guo JJ, Liu YJ (2002) Preliminary study of Precambrian geology in the north Tibet-Qinghai Plateau. Geological Publishing House, Beijing, pp. 1–130 **(in Chinese with English abstract)**.

Lu L, Wu ZH, Hu DG, Barosh PJ, Hao S, Zhou CJ (2010) Zircon U-Pb age for rhyolite of the Maoniushan Formation and its tectonic significance in the east Kunlun mountains. Acta Petrol Sin 26(4): 1150–1158 **(in Chinese with English abstract)**. https://doi.org/10.3724/SP.J.1084.2010.00199

Ludwig KR (2003) Isoplot 3.0–a geochronological toolkit for microsoft Excel. Berkeley Geochronol Center Spec Publ 4:1–70

Luo ZH, Ke S, Cao YQ, Deng JF, Chen HW (2002) Late Indosinian mantle-derived magmatism in the East Kunlun. Geol Bull China 21(6):292–297 ((**in Chinese with English abstract**))

Ma CQ, Xiong FH, Yin S, Wang LX, Gao K (2015) Intensity and cyclicity of orogenic magmatism: an example from a Paleo-Tethyan granitoid batholith, Eastern Kunlun. Northern Qinghai-Tibetan Plateau. Acta Petrol Sin 31(12):3555–3568 ((**in Chinese with English abstract**))

Martin H (1999) Adakitic magmas: modern analogues of Archaean granitoids. Lithos 46(3):411–429. https://doi.org/10.1016/S0024-4937(98)00076-0

McCulloch MT, Gamble JA (1991) Geochemical and geodynamical constraints on subduction zone magmatism. Earth Planet Sci Lett 102(3–4):358–374. https://doi.org/10.1016/0012-821X(91)90029-H

Meng FC, Jia LH, Ren YF, Liu Q, Duan XP (2017) Magmatic and metamorphic events recorded in the gneisses of the Wenquan region, East Kunlun Mountains, Northwest China: evidence from the zircon U-Pb geochronology. Acta Petrol Sin 33(12): 3691–3709 **(in Chinese with English abstract)**. https://doi.org/10.1186/s40064-014-0778-5

Middlemost EAK (1994) Naming materials in the magma/igneous rock system. Earth-Sci Rev 37(3–4):215–224. https://doi.org/10.1016/0012-8252(94)90029-93-4

Mo XX (2010) A review and prospect of geological researches on the Qinghai-Tibet Plateau. Geol China 37(4):841–853 ((**in Chinese with English abstract**))

Mo XX, Luo ZH, Deng JF, Yu XH, Liu CD, Chen HW, Yuan WM, Liu YH (2007) Granitoids and crustal growth in the East-Kunlun orogenic belt. Geol J Chin Uni 13(3):403–414 ((**in Chinese with English abstract**))

Molnar P, Burchfiel BC, Zhao ZY, Liang KY, Wang SJ, Huang MM (1987) Geologic evolution of northern Tibet: results of an expedition to Ulugh Muztagh. Science 235(4786):299–305. https://doi.org/10.1126/science.235.4786.299

Mu DL, Li SZ, Wang Q, Somerville I, Wang YH, Zhao SJ, Li XY, Yu SY, Suo YH (2018) Early Paleozoic Orocline in the Central China Orogen. Gondwana Res 63:85–104. https://doi.org/10.1016/j.gr.2018.04.019

Pan GT, Wang LQ, Li RS, Yuan SH, Ji WH, Yin FG, Zhang WP, Wang BD (2012) Tectonic evolution of the Qinghai-Tibet Plateau. J Asian Earth Sci 53:3–14. https://doi.org/10.1016/j.jseaes.2011.12.018

Patino-Douce AE, Johnston AD (1991) Phase equilibria and melt productivity in the pelitic system: implications for the origin of peraluminous granitoids and aluminous granulites. Contrib to Mineral Petrol 107(2):202–218. https://doi.org/10.1007/BF00310707

Pearce JA (1996) Sources and setting of granitic rocks. Episodes 19(4):120–125. https://doi.org/10.18814/epiiugs/1996/v19i4/005

Pearce JA, Norry MJ (1979) Petrogenetic implications of Ti, Zr, Y, and Nb variations in volcanic rocks. Contrib to Mineral Petrol 69:33–47. https://doi.org/10.1007/BF00375192

Pearce JA, Harris NBW, Tindle AG (1984) Trace element discrimination diagrams for the tectonic interpretation of granitic rocks. J Petrol 25:956–983. https://doi.org/10.1093/petrology/25.4.956

Pei XZ (2001) Geological evolution and dynamics of the Miaulue-A'nyemaqen tectonic zone, central China. Northwest University (Ph. D thesis): 1–155 **(in Chinese with English abstract)**.

Pei XZ, Hu N, Liu CJ, Li RB, Li ZC, Chen YX, Pei L, Liu ZQ, Chen GC, Yang J (2015) Detrital composition, geochemical characteristics and provenance analysis for the maerzheng formation sandstone in Gerizhuotuo area, southern margin of East Kunlun Region. Geol Rev 61(2):307–323 ((**in Chinese with English abstract**))

Pei L, Li RB, Pei XZ, Liu JL, Li ZC, Liu CJ, Chen YX, Liu ZQ, Chen GC, Hu N, Gao F (2017) Sediment source analysis for the Maérzheng Formation Sandstone in Gerizhuotuo Area, Southern Margin of East Kunlun Region: evidence for Detrital Zircon U-Pb Geochronology. Acta Geol Sin 91(6):1326–1344 ((**in Chinese with English abstract**))

Pei XZ, Li RB, Li ZC, Liu CJ, Chen YX, Pei L, Liu ZQ, Chen GC, Li XB, Wang M (2018) Composition feature and formation process of Buqingshan Composite Accretionary Mélange Belt in southern margin of East Kunlun Orogen. Earth Sci 43(12): 4498–4520 **(in Chinese with English abstract)**. https://doi.org/10.3799/dqkx.2018.124

Qinghai Geological Bureau (1972) 1:200000 Alakehu Regional Geological Survey Report, unpublished **(in Chinese)**.

Ren JS (2004) Some problems on the Kunlun-Qinling orogenic system. Northwest Geol 37(1):1–5 ((**in Chinese with English abstract**))

Rickwood PC (1989) Boundary lines within petrologic diagrams which use oxides of major and minor elements. Lithos 22(4):247–263. https://doi.org/10.1016/0024-4937(89)90028-5

Siebel W, Blaha U, Chen FK, Johann R (2005) Geochronology and geochemistry of a dyke-host rock association and implications for the formation of the Bavarian Pfahl shear zone, Bohemian

massif. Int J Earth Sci 94 (1): 8–23. https://doi.org/10.1007/s00531-004-0445-0

Sisson TW, Ratajeski K, Hankins WB, Glazner AF (2005) Voluminous granitic Magmas from common basaltic sources. Contrib Min Petrol 148(5):635–661. https://doi.org/10.1007/s00410-004-0632-9

Söderlund U, Patchett PJ, Vervoort JD, Isachsen CE (2004) The ^{176}Lu decay constant determined by Lu-Hf and U-Pb isotope systematics of Precambrian mafic intrusions. Earth Planet Sci Lett 219(3–4):311–324. https://doi.org/10.1016/S0012-821X(04)00012-3

Stern CR, Kilian R (1996) Role of subducted slab, mantle wedge and continental crust in the generation of adakites from the Andean Austral Volcanic Zone. Contrib Mineral Petrol 123: 263–281. https://doi.org/10.1007/s004100050155

Sun SS, McDonough WF (1989) Chemical and isotopic systematics of ocean basins: Implications for mantle composition and processes. In: Saunders AD, Norry MJ (eds) Magmatism of the ocean basins. Geological Society Special Publication London 42(1): 313–345. https://doi.org/10.1144/GSL.SP.1989.042.01.19

Sun Y, Pei XZ, Ding SP, Li RB, Feng JY, Zhang YF, Li ZC, Chen YX, Zhang XF, Chen GC (2009) Halagatu magma mixing granite in the East Kunlun mountains: evidence from zircon U-Pb dating. Acta Geol Sin 83(7):1000–1010 ((**in Chinese with English abstract**))

Sylvester PJ (1998) Post-collisional strongly peraluminous granites. Lithos 45:29–44. https://doi.org/10.1016/S0024-4937(98)00024-3

Taylor SR, McLennan SM (1985) The continental crust: its composition and evolution. Blackwell Scientific Publication, Carlton, pp. 312. https://doi.org/10.1016/0031-9201(86)90093-2

Vervoort JD, Patchett PJ, Gehrels GE, Nulman AP (1996) Constraints on early Earth differentiation from hafnium and neodymium isotopes. Nature 379:624–627. https://doi.org/10.1038/379624a0

Wang YB, Yang H (2004) Middle Permian palaeobiogeography study in east Kunlun, A'nyêmaqên and Bayan Har. Sci China Ser D Earth Sci 47(12):1120–1126. https://doi.org/10.1360/02yd0450

Wang GC, Wang QH, Jian P, Zhu YH (2004) Zircon SHRIMP ages of Precambrian metamorphic basement rocks and their tectonic significance in the eastern Kunlun Mountains, Qinghai Province, China. Earth Sci Front 11 (4): 481–490 **(in Chinese with English abstract)**. https://doi.org/10.1007/BF02873097

Wang Q, Zhao J, Zhang CL, Yu SY, Ye XT, Liu XQ (2022) Paleozoic post-collisional magmatism and high-temperature granulite-facies metamorphism coupling with lithospheric delamination of the East Kunlun Orogenic Belt NW China. Geosci Front 13:101271. https://doi.org/10.1016/j.gsf.2021.101271

Wolf MB, Wyllie PJ (1989) The formation of tonalitic liquids during the vapor-absent partial melting of amphibolite at 10 kbar. EOS Trans Am Geophys Union 70:506–518

Wu YB, Zheng YF (2004) Genesis of zircon and its constraints on interpretation of U-Pb age. Chin Sci Bull 49(15):1554–1569. https://doi.org/10.1007/BF03184122

Wu FY, Yang YH, Xie LW, Yang JH, Xu P (2006) Hf isotopic compositions of the standard zircons and baddeleyites used in U-Pb geochronology. Chem Geol 234(1–2):105–126. https://doi.org/10.1016/j.chemgeo.2006.05.003

Wu FY, Li XH, Zheng YF, Gao S (2007) Lu-Hf isotopic systematics and their applications in petrology. Acta Petrol Sin 23(2): 185–220 **(in Chinese with English abstract)**. https://doi.org/10.1016/j.sedgeo.2006.03.028

Xiong FH, Ma CQ, Jiang HA, Liu B, Huang J (2014) Geochronology and geochemistry of middle Devonian mafic dykes in the East Kunlun orogenic belt, northern Tibet Plateau: Implications for the transition from Prototethys to Paleotethys orogeny. Geochemistry 74(2):225–235. https://doi.org/10.1016/j.chemer.2013.07.004

Xiong FH, Ma CQ, Wu L, Jiang HA, Liu B (2015) Geochemistry, zircon U-Pb ages and Sr-Nd-Hf isotopes of an Ordovician appinitic pluton in the East Kunlun orogen: new evidence for Proto-Tethyan subduction. J Asian Earth Sci 111:681–697. https://doi.org/10.1016/j.jseaes.2015.05.025

Xu ZQ, Yang JS, Chen FY (1996) A'nyemaqen suture and subduction-collision dynamics. In: Zhang Q (ed) Study on ophiolites and dynamics. Geological Publishing House, Beijing, pp 185–189 ((**in Chinese with English abstract**))

Xu ZQ, Yang JS, Jiang M, Li HB, Xue GQ, Yuan XC, Qian H (2001) Deep structure and lithospheric shear faults in the east Kunlun-Qiangtang region, northern Tibetan Plateau. Sci China Ser D: Earth Sci 44(Supp): 1–9. https://doi.org/10.1007/BF02911965

Xu ZQ, Yang JS, Li HB, Zhang JX, Wu CL (2007) Orogenic Plateau: Terrane Amalgamation, Collision and Uplift in the Qinghai-Tibet Plateau. Geological Publishing House, Beijing, pp. 1–458 **(in Chinese with English abstract)**.

Xu ZQ, Yang JS, Li WC, Li HQ, Cai ZH, Yan Z, Ma CQ (2013) Paleo-Tethys system and accretionary orogen in the Tibet Plateau. Acta Petrol Sin 29(6):1847–1860 ((**in Chinese with English abstract**))

Yang JS, Robinson PT, Jiang CF, Xu ZQ (1996) Ophiolites of the Kunlun mountains, China and their tectonic implications. Tectonophysics 258(1–4):215–231. https://doi.org/10.1016/0040-1951(95)00199-9

Yang JS, Wang XB, Shi RD, Xu ZQ, Wu CL (2004) The Dur'ngoi ophiolite in east Kunlun, northern Qinghai-Tibet Plateau: a fragment of Paleo-Tethyan oceanic crust. Geol China 31(3):225–238 ((**in Chinese with English abstract**))

Yang JS, Xu ZQ, Li HB, Shi RD (2005) The Paleo-Tethyan volcanism and plate tectonic regime in the A'nyemaqen region of East Kunlun, Northern Tibet Plateau. Acta Petrol et Mineral 24(5):369–380 ((**in Chinese with English abstract**))

Yang JS, Xu ZQ, Li ZL, Xu XZ, Li TF, Ren YF, Li HQ, Chen SY, Robinson PT (2009) Discovery of an eclogite belt in the Lhasa block, Tibet: a new border for Paleo-Tethys? J Asian Earth Sci 34(1):76–89. https://doi.org/10.1016/j.jseaes.2008.04.001

Yang J, Pei XZ, Li RB, Li ZC, Liu ZQ, Pei L, Liu CJ, Chen YX, Chen GC, Gao JM (2014) Geochemical characteristics and geological implications of Haerguole basalt in Buqingshan area on the southern margin of East Kunlun Mountains. Geol China 41(2):335–350 ((**in Chinese with English abstract**))

Yang S, Pei XZ, Li RB, Liu CJ, Chen YX, Li ZC, Wang XB, Sang JZ, Chen G, Deng WB (2016) Provenance analysis and structural implications of Gequ Formation at the Buqingshan area in the eastern segment of the East Kunlun region. Geol Bull China 35(5):674–686 ((**in Chinese with English abstract**))

Yin HF, Zhang KX (1997) Characteristics of the Eastern Kunlun Orogenic Belt. Earth Sci 22:339–342 ((**in Chinese with English abstract**))

Yin HF, Zhang KX (2003) Regional geological report of the Peoples Republic of China: Donggi Conag Hu map, scale 1 : 250000. China University of Geosciences Press, Wuhan, pp. 1–457 **(in Chinese)**.

Yu M, Dick JM, Feng CY, Li B, Wang H (2020) The tectonic evolution of the East Kunlun Orogen, northern Tibetan Plateau: a critical review with an integrated geodynamic model. J Asian Earth Sci 191:104168. https://doi.org/10.1016/j.jseaes.2019.104168

Yuan HL, Wu FY, Gao S, Liu XM, Xu P, Sun DY (2003) Determination of U-Pb age and rare earth element concentrations of zircons from Cenozoic intrusions in northeastern China by laser ablation ICP-MS. Chin Sci Bull 48(22):2411–2421. https://doi.org/10.1360/03wd0139

Yuan HL, Gao S, Liu XM, Li HM, Günther D, Wu FY (2004) Accurate U-Pb age and trace element determinations of zircon by laser ablation-Inductively coupled plasma mass spectrometry.

Geostand Geoanal Res 28(3):353–370. https://doi.org/10.1111/j.1751-908X.2004.tb00755.x

Yuan HL, Gao S, Dai MN, Zong CL, Gunther D, Fontaine GH, Liu XM, Diwu CR (2008) Simultaneous determinations of U-Pb age, Hf isotopes and trace element compositions of zircon by excimer laser-ablation quadrupole and multiple-collector ICP-MS. Chem Geol 247(1–2):100–118. https://doi.org/10.1016/j.chemgeo.2007.10.003

Zhang YF (2010) The geological characteristic, age and tectonic setting of Kekesha intrusive rocks of Early Paleozoic in Dulan county og the East Kunlun area. Chang'an University (Master thesis): 1–83 **(in Chinese with English abstract)**.

Zhang KX, Huang JC, Luo MS, Zhang TP, Bai YS (1999) Sedimentary geochemical features of A'nimaqing mélange zone in eastern Kunlun mountains. Earth Sci 24(2):111–115 ((**in Chinese with English abstract**))

Zhang KX, Huang JC, Yin HF, Wang GC, Wang YB, Feng QH, Tian J (2000) Application of radiolarians and other fossils in non-Smith strata: exemplified by the A'nyêmaqên mélange belt in east Kunlun Mts. Sci China Ser D Earth Sci 43(4):364–374. https://doi.org/10.1007/BF02959447

Zhang GW, Dong YP, Lai SC, Guo AL, Meng QR, Liu SF, Cheng SY, Yao AP, Zhang ZQ, Pei XZ, Li SZ (2004) Mianlüe tectonic zone and Mianlüe suture zone on southern margin of Qinling-Dabie orogenic belt. Sci China Ser D Earth Sci 47(4):300–316. https://doi.org/10.1360/02YD0526

Zhang YF, Pei XZ, Ding SP, Li RB, Feng JY, Sun Y, Li ZC, Chen YX (2010a) LA-ICP-MS zircon U-Pb age of quartz diorite at the Kekesha area of Dulan County, eastern section of the East Kunlun orogenic belt, China and its significance. Geol Bull China 29(1):79–85 ((**in Chinese with English abstract**))

Zhang YL, Hu DG, Shi YR, Lu L (2010b) SHRIMP zircon U-Pb ages and tectonic significance of Maoniushan Formation volcanic rocks in east Kunlun orogenic belt China. Geol Bull China 29(11):1614–1618 ((**in Chinese with English abstract**))

Zhao X, Fu LB, Wei JH, Bagas L, Santosh M, Liu Y, Zhang DH, Zhou HZ (2019) Late Permian back-arc extension of the eastern Paleo-Tethys Ocean: evidence from the East Kunlun Orogen, Northern Tibetan Plateau. Lithos 340–341:34–48. https://doi.org/10.1016/j.lithos.2019.05.006

Zheng YF, Zhang SB, Zhao ZF, Wu YB, Li XH, Li ZX, Wu FY (2007) Contrasting zircon Hf and O isotopes in the two episodes of Neoproterozoic granitoids in South China: implications for growth and reworking of continental crust. Lithos 96(1–2):127–150. https://doi.org/10.1016/j.lithos.2006.10.003

Zhou HZ, Zhang DH, Wei JH, Wang DZ, Santosh M, Shi WJ, Chen JJ, Zhao X (2020) Petrogenesis of Late Triassic mafic enclaves and host granodiorite in the Eastern Kunlun Orogenic Belt, China: implications for the reworking of juvenile crust by delamination-induced asthenosphere upwelling. Gondwana Res 84:52–70. https://doi.org/10.1016/j.gr.2020.02.012

Zhu YH, Zhang KX, Pan YM, Chen NS, Wang GC, Hou GJ (1999) Determination of different ophiolitic belts in eastern Kunlun orogenic zone and their tectonic significance. Earth Sci 24(2):134–138 ((**in Chinese with English abstract**))

Zhu YH, Zhang KX, Wang GC (2002) Evolution of ophiolite, magma and tectonic magma in eastern Kunlun compound orogenic belt. China University of Geosciences Press, Wuhan, pp. 104–105 **(in Chinese with English abstract)**.

Zhu YH, Lin QX, Jia CX, Wang GC (2006) SHRIMP zircon U-Pb age and significance of early Paleozoic volcanic rocks in east Kunlun orogenic belt, Qinghai province, China. Sci China Ser D Earth Sci 49(1):88–96. https://doi.org/10.1007/s11430-004-5317-8